Undergraduate's Internship Program

ORCA - Energy Reconstruction Studies

Department of Physics
Aristotle University of Thessaloniki

Michael Chadolias

Thessaloniki, March 9, 2022

Submitted in partial fulfillment of the requirements for the degree of B. Sc. in Physics
Supervised by Dr Katerina Tzamarioudaki

Abstract

This report covers the work accomplished accomplished as part of the generic elective course **AME501 Internship** of the *B.S in Physics from AUTh University*. The internship was performed in NCSR Democritus in the Institute of Nuclear and Particle Physics in the *Astroparticle Research Group*, which is a member of the *KM3NeT Collaboration*. The research was carried out under the guidance of Dr Ekaterini Tzamarioudaki and the invaluable help of Phd Candidate Dimitrios Stavropoulos. Data collected with the KM3NeT-ORCA detector have been used for this study. The energy resolution for reconstructed muon tracks originating from neutrino interactions has been investigated. For the study an individual code, analyze_orca6_data.cc(A). Many variables were taken into consideration like the position of the vertex, the 3D direction of the incident neutrino, the energy of the neutrino and the proportion of the energy in the daughter particle (muon). These studies are presented in detail in the following report.

Contents

List of Figures

1. Introduction

The Standard Model is the best description of the subatomic world. It contains the 12 known particles, their antiparticles, three fundamental forces with their 4 gauge bosons, and generates mass using a single scalar boson [11]. The theory results from many years of theoretical and experimental research and has predicted the existence of new particles, such as the W ± /Z bosons, gluon, and the Higgs.

The current neutrino oscillation framework comprises three flavours (ν_e, ν_μ, ν_τ) and three mass eigenstates (ν_1, ν_2, ν_3), although it is still an open question whether more non- interacting neutrinos exist[20]. E ν and L, and a set of constants determine the mixing probability. Most of them are contained within the PMNS matrix[20], which parametrises the mixing using three mixing angles and one CP violating phase, similar to the quark sector.

$$U = \begin{pmatrix} 1 & 0 & 0 \\ 0 & c_{23} & s_{23} \\ 0 & -s_{23} & c_{23} \end{pmatrix} * \begin{pmatrix} c_{13} & 0 & e^{-i\delta}s_{13} \\ 0 & 1 & 0 \\ -e^{-i\delta}s_{13} & 0 & c_{13} \end{pmatrix} * \begin{pmatrix} c_{12} & s_{12} & 0 \\ -s_{12} & c_{12} & 0 \\ 0 & 0 & 1 \end{pmatrix} \tag{1.1}$$

The other constants are the squared mass differences between the mass eigenstates. With three eigenstates, two mass differences are independent. So far, experiments are unable to measure the sign of one of the mass differences, which results in a degeneracy in the mass ordering. This is known as the Mass Hierarchy problem, also named the Mass Ordering problem. A promising method for determining the neutrino mass ordering is to exploit the effect of matter on the oscillation probability of neutrinos and antineutrinos[2], which alters the oscillation probability depending on energy, distance travelled, and the electron density of the matter traversed.

The ORCA (Oscillation Research with Cosmics in the Abyss) telescope of the KM3NeT (Cubic Kilometer Neutrino telescope) infrastructures plans to use this method with neutrinos and antineutrinos produced by cosmic rays. Cosmic rays are highly energetic charged particles that hit the atmosphere and create a shower of particles including ν e/μ and ν e/μ . These atmospheric neutrinos oscillate through the Earth and create high-energy interaction products, such as muons, taus, and electrons. The aim of the experiment is to find the correct hierarchy of the masses of the neutrinos, more information will be presented in a following paragraph **(ref)**. Unfortunately, the detector outside the operational range of the experiment experiences some inconsistencies with the reconstruction of the energy of the incumbent particle. Even though this problem doesn't affect the collaboration, since it has released its first oscillation measurement[17] with a confidence level of 5.9σ over the non-oscillation scenario.

ORCA's detector structure due to its scientific goal is optimised for a few GeV , where matter effects have a strong presence. It is, however, unable to distinguish between neutrino flavour of the interaction directly. Instead, the detector can only separate two interaction signatures: showers and tracks (**Section:3.3.2**). In this report focuses in the reconstruction of energy for the current detector lay-out of six strings. The report starts with a description of neutrino oscillations and the KM3NeT detector in **Chapter 2,3** respectively. Furthermore, the reconstruction of energy and track for the ORCA detector are defined in **chapter 4**. In **chapter5**, the current quality reconstruction is clarified along with the methodology of the analysis trying to interpret it. In **chapter6**, the results from the various tools that were utilized is presented. **Chapter 7** finishes the report with a discussion of the results and the conclusion.

2. Neutrino Oscillations

In this chapter we shall discuss neutrino physics. Neutrinos produced with a certain flavour, $\nu_e, \nu_\mu or \nu_\tau$, may be detected later with a different flavour, if enough time is left between production and detection. Consequently $\nu_e, \nu_\mu or \nu_\tau$ are not stationary states with definite mass, but superpositions of them. Neutrinos can change flavour by two mechanisms: oscillations and matter effects.

2.1 History of the neutrino

The idea for a neutrino was first, formulated by Wolfgang Pauli in for the process of β^- decay. The nucleus changes charge from Z to Z + 1 alongside the emission of an electron depicted in (ref). Given the fact that it is a two-body decay, the energy of the electron would be constant. However, the experiments have shown an continuous spectrum.

$$A(N, Z) \leftarrow A(N - 1, Z + 1) + \eta^- \tag{2.1}$$

Through the theory and calculations of Pauli, showed that cross sections of the supposed particles, neutrinos, were very small in order to be detected. With the advancement of experimental instrumentation and the invention of higher fluxes of neutrinos. In 1956, Reines and Cowan successfully measured a neutrino interaction using inverse beta decay (2.2) for the first time [9]. An electron antineutrino from the nuclear reactor interacts with a proton and emits a positron and neutron. The positron immediately annihilates with electrons in the medium to photons, while a nucleus captures the neutron and emits delayed light allowing for background reduction

$$\nu + p \rightarrow \eta^+ + n \tag{2.2}$$

From the electron neutrino discovery, only six years took to find the muon neutrino, from cosmic radiation and pion decays. The tau lepton was the third and final flavour discovered in the DELPHI, Cern experiment through the Z boson decay. In order to detect the tau neutrino interaction, we had to wait until 2000 with the DONUT collaboration.

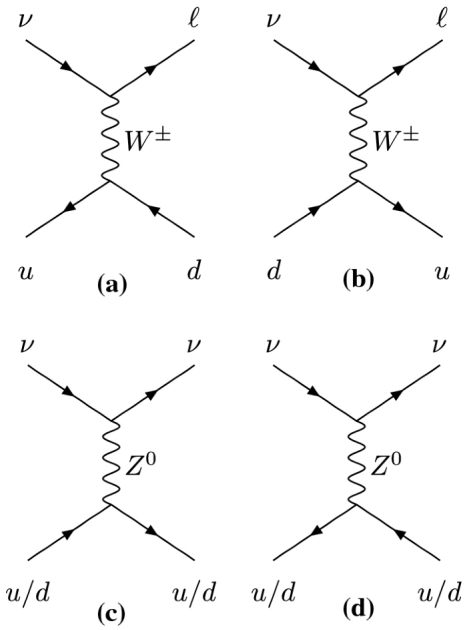

Figure 2.1: CC neutrino (a), CC anti-neutrino (b) and NC (c-d) interactions [16]

2.2 Neutrino oscillation

Two-neutrino mixing and flavour oscillations in vacuum were introduced in (ref). In this section, we present the standard parametrisation of three-neutrino mixing, extend the derivation of vacuum oscillation probabilities for three flavours, and discuss the important differences with the two-neutrino case.

Accoding to [5], the leptonic charged current is written as:

$$j^{\mu}_{CC,lep} = 2 \sum_{a=e,\mu,\tau} \nu_{aL} \gamma^{\mu} l_{a,L} = \nu_L U^{\dagger} \gamma^{\mu} l_L \tag{2.3}$$

with the mixing matrix U:

$$U = V_L^{l\dagger} V_L^{\nu} \tag{2.4}$$

The left-handed flavour neutrino fields $\nu_{eL}, \nu_{\mu L}, \nu_{\tau L}$ which couple directly with the charged leptons of the corresponding generation in the weak CC interaction are therefore:

$$\begin{pmatrix} \nu_{eL} \\ \nu_{\mu L} \\ \nu_{\tau L} \end{pmatrix} \equiv U \begin{pmatrix} \nu_{1L} \\ \nu_{2L} \\ \nu_{3L} \end{pmatrix} = \begin{pmatrix} U_{e1} & U_{e2} & U_{e3} \\ U_{\mu 1} & U_{\mu 2} & U_{\mu 3} \\ U_{\tau 1} & U_{\tau 2} & U_{\tau 3} \end{pmatrix} \begin{pmatrix} \nu_{1L} \\ \nu_{2L} \\ \nu_{3L} \end{pmatrix} \tag{2.5}$$

For the right handed components of the neutrinos, it is not needed to solve the weak CC interaction since they can't couple with charged leptons [20]. The mixing matrix U is called the Pontecorvo-Maki-Nakagawa-Sakata (PMNS) matrix. It can be decomposed into a product of three real rotation matrices, parametrized by mixing angles θ_{12}, θ_{13} and θ_{23}, and a diagonal matrix involving a complex phase $e^{i\delta}CP$.

The standard parametrisation of the PMNS matrix is:

$$U = \begin{pmatrix} 1 & 0 & 0 \\ 0 & c_{23} & s_{23} \\ 0 & -s_{23} & c_{23} \end{pmatrix} * \begin{pmatrix} c_{13} & 0 & e^{-i\delta}s_{13} \\ 0 & 1 & 0 \\ -e^{-i\delta}s_{13} & 0 & c_{13} \end{pmatrix} * \begin{pmatrix} c_{12} & s_{12} & 0 \\ -s_{12} & c_{12} & 0 \\ 0 & 0 & 1 \end{pmatrix} \tag{2.6}$$

with the short notations

$$c_{ij} = \cos\theta_{ij}, s_{ij} = \sin\theta_{ij}$$

The mixing angles can be chosen in the interval of 0 to $\pi/2$.

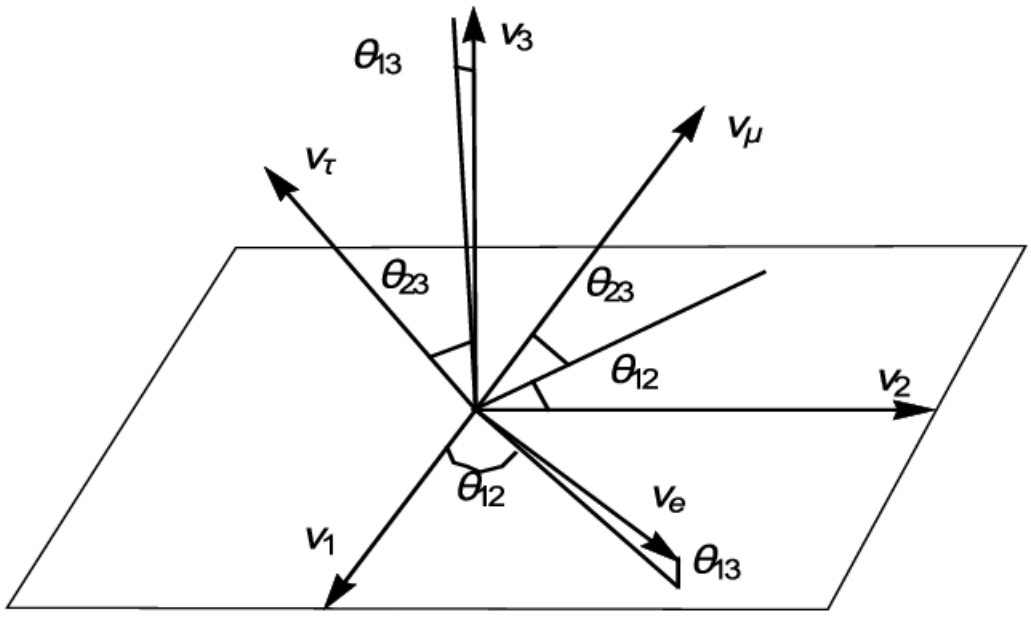

Figure 2.2: Neutrino mixing angles [12]

Neutrino oscillations in vacuum are then controlled by the following six independent parameters:

$$\theta_{12}, \theta_{13}, \theta_{23}, \delta_{CP}, \Delta m^2_{21}, \Delta m^2_{31}$$

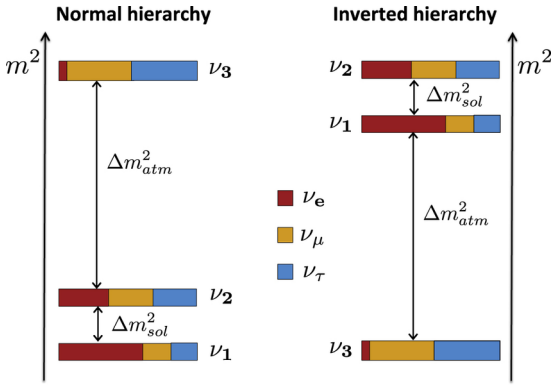

Figure 2.3: Scheme of the two distinct neutrino mass hierarchies [1]

2.3 Measuring neutrino mass hierarchy

Even though, there were many experiments, the mass hierarchy has not been determined so far. After fixing $\Delta m^2_{21} = (\Delta m^2)_{sol} > 0$, two solutions remain possible depending on the sign of Δm^2_{31}: the normal hierarchy (NH:m1 $<$ m2 $<$ m3) and the inverted hierarchy (IH: m3 $<$ m1 $<$ m2), as seen in [1]. It is paramount from a theoretical standpoint, to determine the neutrino mass hierarchy, to constrain the models that seek to explain the origin of mass in the lepton sector.

According to [18], (2.4) summarizes the present knowledge of neutrino masses and mixings including neutrino mixing angles, the CP phase $\delta_C P$, and neutrino mass-squared differences $\Delta m^2_{ij} = m^2_i m^2_j$, based on the recent fit [13] after the Neutrino 2014.

Parameter	Best fit value $\pm 1\sigma$	3σ range
$\sin^2\theta_{12}$	$0.304^{+0.012}_{-0.012}$	(0.270, 0.344)
θ_{12} (degrees)	$33.48^{+0.77}_{-0.74}$	(31.30, 35.90)
$\sin^2\theta_{23}$	$[0.451^{+0.001}_{-0.001}]$ or $0.577^{+0.027}_{-0.035}$	(0.385, 0.644)
θ_{23} (degrees)	$[42.2^{+0.1}_{-0.1}]$ or $49.4^{+1.6}_{-2.0}$	(38.4, 53.3)
$\sin^2\theta_{13}$	$0.0219^{+0.0010}_{-0.0011}$	(0.0188, 0.0251)
θ_{13} (degrees)	$8.52^{+0.20}_{-0.21}$	(7.87, 9.11)
δ_{CP} (degrees)	251^{+67}_{-59}	(0, 360)
$\Delta m^2_{21} \times 10^{-5}$ eV^2	$7.50^{+0.19}_{-0.17}$	(7.03, 8.09)
(normal) $\Delta m^2_{31} \times 10^{-3}$ eV^2	$+2.458^{+0.046}_{-0.047}$	(+2.325, +2.599)
(inverted) $\Delta m^2_{32} \times 10^{-3}$ eV^2	$-2.448^{+0.047}_{-0.047}$	(−2.590, −2.307)

Figure 2.4: Possible parameters for NH and IH

3. KM3NET - Infrastructure

KM3NeT is a research collaboration of various academic institutions through out the world joined together to house the next generation neutrino telescopes. Located in the deep-water parts of the Mediterranean, two different experiments will be carried out in order to study the properties of neutrino particles. With the ARCA telescope, KM3NeT scientists will search for neutrinos from distant astrophysical sources such as supernovae, gamma ray bursters or colliding stars. The ORCA telescope is the instrument for KM3NeT scientists studying neutrino properties exploiting neutrinos generated in the Earth's atmosphere. The KM3NeT project, as others similar scientific projects like IceCube, ANTARES, Baikal-GVD, utilizes optical module design technology.

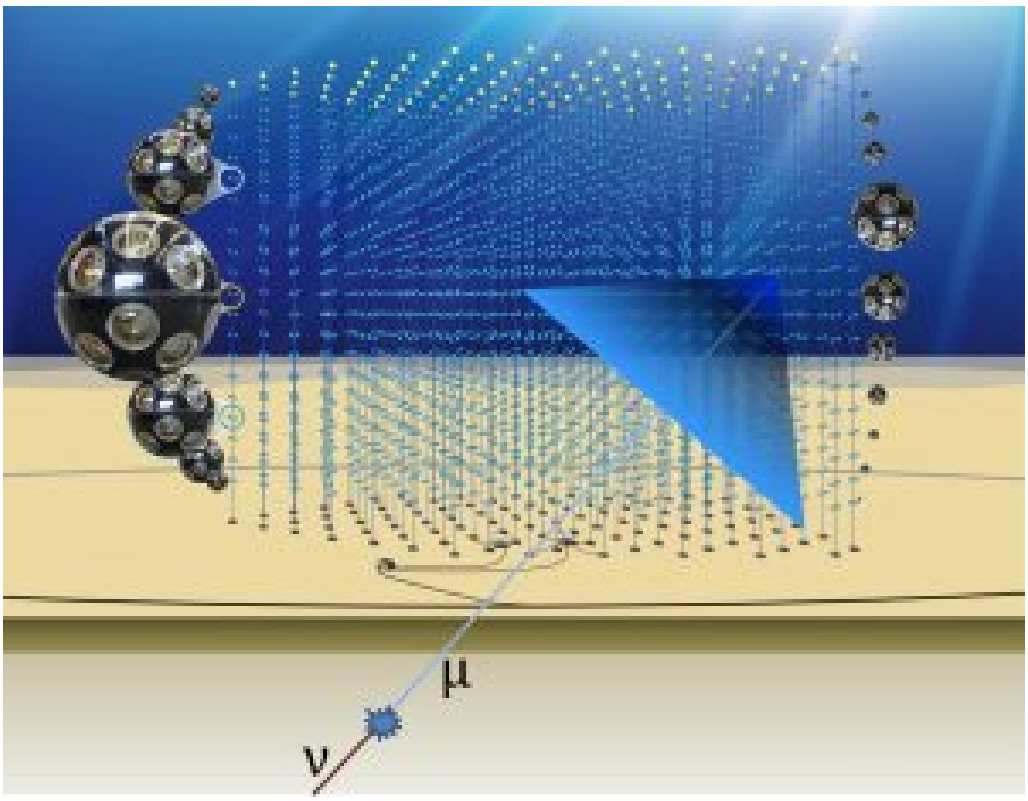

Figure 3.1: Artistic Representation of KM3NeT. Source: **official site**.

3.1 KM3NeT

3.1.1 Neutrino telescopes

Neutrino detectors require large detector volumes in order to detect a considerable amount of neutrinos, due to the small cross sections. The concept of neutrino telescopes appeared in 1961 when Markov proposed using the water of deep lakes or the sea to detect the secondary muons created in the CC interaction of high-energy neutrinos[3]. These water-based detectors register the Cherenkov light from the secondary particles in order to be detected by photo-multipliers. From the arrival time of the Cherenkov photons and the positions of the photosensors, the direction and the energy of the incoming neutrino to the neutrino interaction can be retrieved.

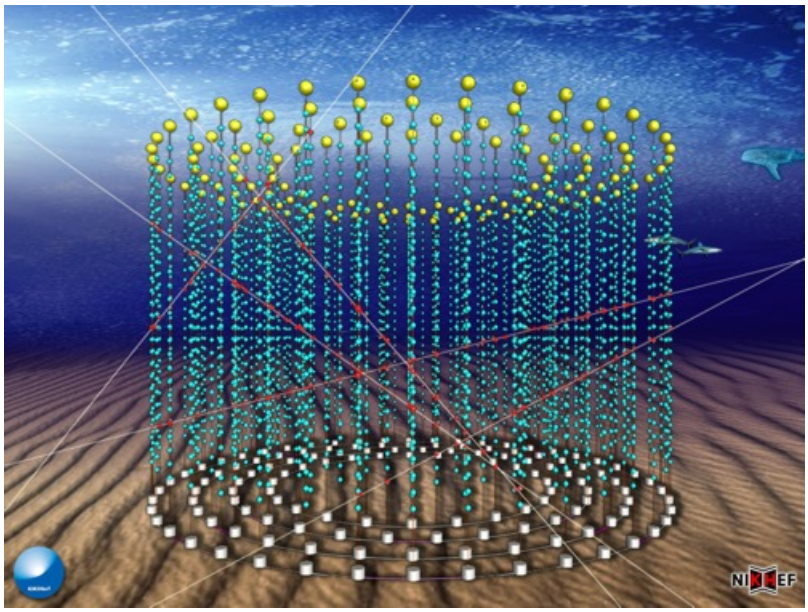

The Neutrino detectors use the earth as an background in order to reduce contamination from atmospheric muons produced in air-showers resulting from cosmic-ray interactions. That's why the experiments are placed in the deep-ocean like KM3NeT, Baikal, ANTARES and IceCube or underground location like SuperKamiokade and Gran Sasso. Their main difference is the photocathode area density, which determines in particular the neutrino energy threshold, and is optimised for the targeted physics goal.

3.1.2 KM3NeT-ARCA Site

The ARCA (Atroparticle Research with Cosmics in the Abyss) is located 100km offshore from Porto Palo di Capo Passero, Sicily, Italy at depth of 3500m. The site used to be the former NEMO site. With a primary aim of ARCA[1] of studying high-energy galactic neutrinos. Given

its location it can observe up-going neutrinos from most of the Galactic Plane, including the Galactic Centre.The KM3NeT/ARCA detector, optimised for the neutrino energy range from few TeV to 100 PeV, focuses on high-energy neutrino astrophysics.

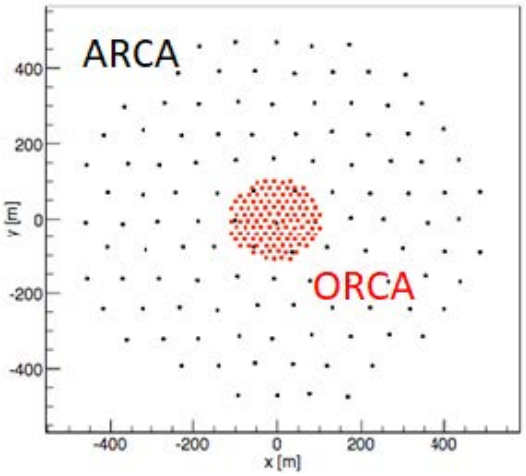

Figure 3.2: (Left) photo of a the footprint between the two detectors. (Right) relative size of the detectors. Source: **official site**.

The KM3NeT-ARCA detector[19], is an an array of photomultiplier tubes (PMTs), capable of detecting neutrino events via the Cherenkov radiation emitted by the daughter particles. The DOMs are tied together in groups of 18 forming vertical structures, the so-called Detection Units. Each DU is anchored to the seabed and remain vertical due to the buoyancy of the DOMs as well as of abuoy which is tied on its top. The vertical distance between the DOMs in a DU is 36 m, and the horizontal distance between the DUs is 90 m.

3.1.3 KM3NeT-ORCA Site

The ORCA (Oscillation Research with Cosmics in the Abyss) is located 40km offshore Toulon, France at a depth of 2450m. The site is near the ANTARES site. With a primary aim of ORCA measuring the neutrino mass ordering the detector is sensitive to oscillations of atmopheric neutrinos in the energy range of a few GeV. ORCA's detector structure is optimised for the 3 to 20 GeV range, where matter effects have a strong presence[6].

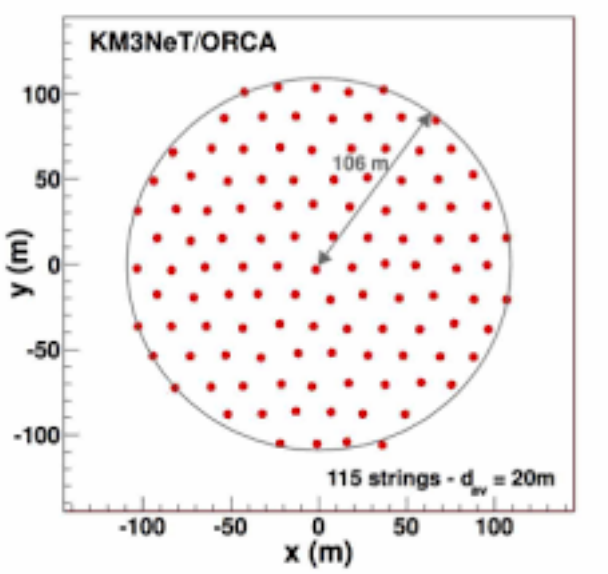

Figure 3.3: Bottom-view of ORCA.

Likewise with the KM3NeT/ARCA detector, KM3NeT/ORCA detector is an array of photomultiplier tubes (PMTs), capable of detecting neutrino events via the Cherenkov radiation emmited by the daughter particles. The DOMs are tied together in groups of 18 forming vertical structures, the so-called Detection Units (DUs - Fig.2). Each DU is anchored to the seabed and remain vertical due to the buoyancy of the DOMs as well as of abuoy which is tied on its top. The vertical distance between the DOMs in a DU is 9 m, and the horizontal distance between the DUs is 20 m.

During my internship, the detector consisted of 6 detection units. Therefore, for the analysis I have conducted I have used Monte Carlo simulated events simulated for a detector configuration with 6 Detection Units(ORCA6). As of November 2021, 4 more detection units have been installed. When completed, the ORCA detector will consist of 115 DUs, forming a cylindrical instrumented volume with a radius 100 m, and height 160m [17].

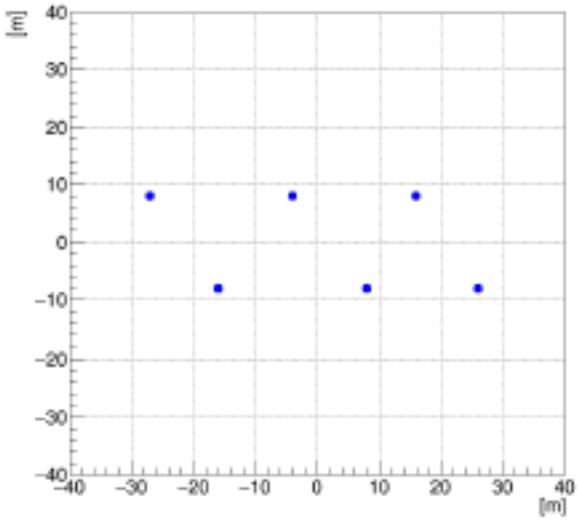

Figure 3.4: Bottom View ORCA6

3.2 Detector Design

3.2.1 Digital Optical Module (DOM)

The KM3NeT digital optical experiment is composed by a transparent spherical vessel that contains inside 31 small-area PMTs[8], along with the associated electronics, calibration components, accessory systems for monitoring and controls. The active part of a neutrino telescope is the optical module. The solution chosen for KM3NeT is based on multi-PMT optical modules, built by means of a large number of small-size PMTs housed in a pressure-resistant glass sphere.

A breakdown structure of the DOM is shown in Figure 2. The internal arrangement has been designed so as to make maximum usage of the available room. The PMTs are equipped with active bases, which allow to have individual control from the shore of the HV and threshold settings for each tube. The bases are equipped with ASICs which perform a digitization of the hits, so that the threshold crossing time and the time-over-threshold can be recorded and sent to shore. The PMTs are installed in a properly shaped support structure. Light collection lenses are installed in front of the PMTs so as to increase the light-sensitive effective area. Optical gel is installed between the PMTs and the glass sphere in order to maximize light transmission. Each DOM acts like an independent measurement node. The system has been designed in such a way that faults taking place in a DOM will not propagate to the other DOMs of the apparatus.

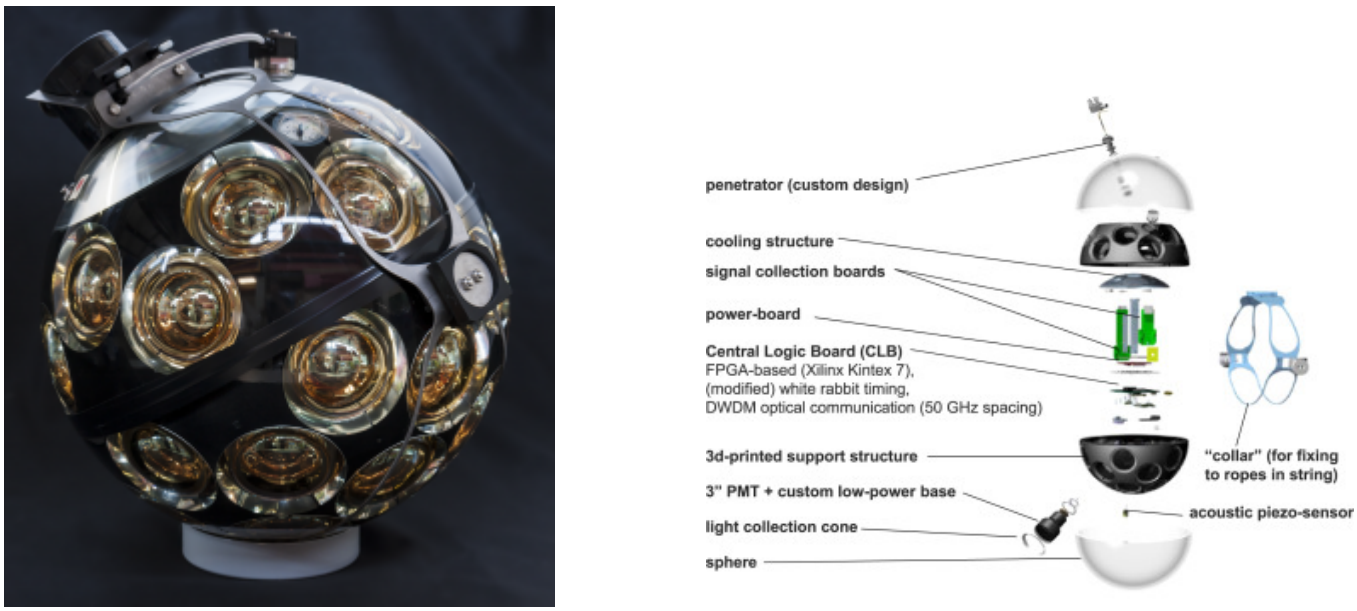

Figure 3.5: Digital Optical Module

3.2.2 Detection String

The detection string is consisted of 18 DOMs [reference]. Depending on the experiment the start of the first DOM from the sea floor, for example the KM3NeT/ARCA is about 80m. Whereas the KM3NET/ORCA is about 40m. Each string comprises two thin (4mm diameter) parallel Dyneema R ropes to which the DOMs are attached via a titanium collar. It is paramount for the normal execution of the experiment that there is no deviation of the DOMs from their initial position of Additional spacers are added in between the DOMs to maintain the ropes parallel. Attached to the ropes is the vertical electro-optical cable, a pressure balanced, oil-filled, plastic tube that contains two copper wires for the power transmission (400 VDC) and 18 optical fibres for the data transmission. At each storey two power conductors and a single fibre are branched out via the breakout box. The breakout box also contains a DC/DC converter (400 V to 12 V).

The power conductors and optical fibre enter the glass sphere via a penetrator. Even though the string design minimises drag and itself is buoyant, additional buoyancy is introduced at the top of the string to reduce the horizontal displacement of the top relative to the base for the case of-large sea currents.

The deployment of the DUs, a large spherical frame is utilized, the so-called launcher vehicle. In the end of the launcher an anchor is used to interact with the seabed, in order to provide stability. The anchor provides space for an interlink cable and a base container, that holds dedicated optical components and an acoustic receiver used for positioning of the detector elements. The principle for the deployment is simple, a surface vessel dynamically provides

(a) Deployment Vessel (b) Launcher vehicle

Figure 3.6: Deployment Procedure

positioning capabilities for the system and releases the launcher. An remotely operated vehicle assists to the connection of the interlink cable from each base to a junction box.

After the anchor reaches the seabed infrastructure due to buoyancy the DOMs are untangled from the launch-vehicle. The empty launcher vehicle floats to the surface and is recovered by the surface vessel. The use of compact strings allows for transportation of many units on board and thus multiple deployments during a single cruise. This method reduces costs and also has advantages in terms of risk reduction

3.3 Detection Principle

From the standard model, it is understood that neutrinos only interact through the weak interaction. Therefore, in order to experimentally detect such a particle, it must be with a secondary product detection. The most preferable method is the interaction of the neutrino with matter.

3.3.1 Cherenkov Emmision

According to the Cherenkov principle, when a charged particle has speed greater than the speed of light in the same dielectric medium spherical Electromagnetic Waves of polarization are generated that follow the motion of the particle. Through the interference of all the above waves a radiation cone is produced. The condition for Cherenkov radiation is the following:

$$v \geq v_{photon} => \beta \geq \frac{1}{n} \tag{3.1}$$

So given that diffraction index is $n = 1.33$ from 3.1 the minimum value for beta for Cherenkov emission is: $\beta_{min} \geq 0.7519$

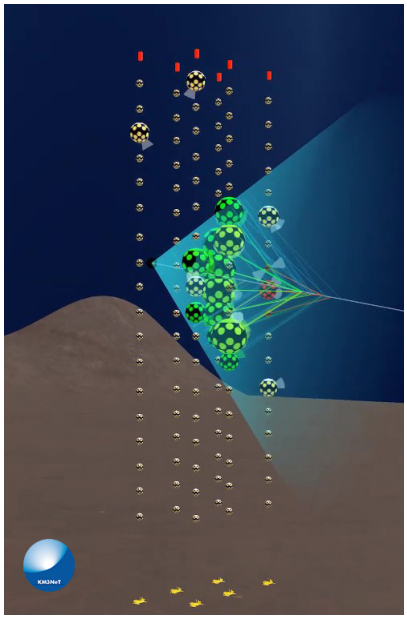

(a) Neutrino Candidate

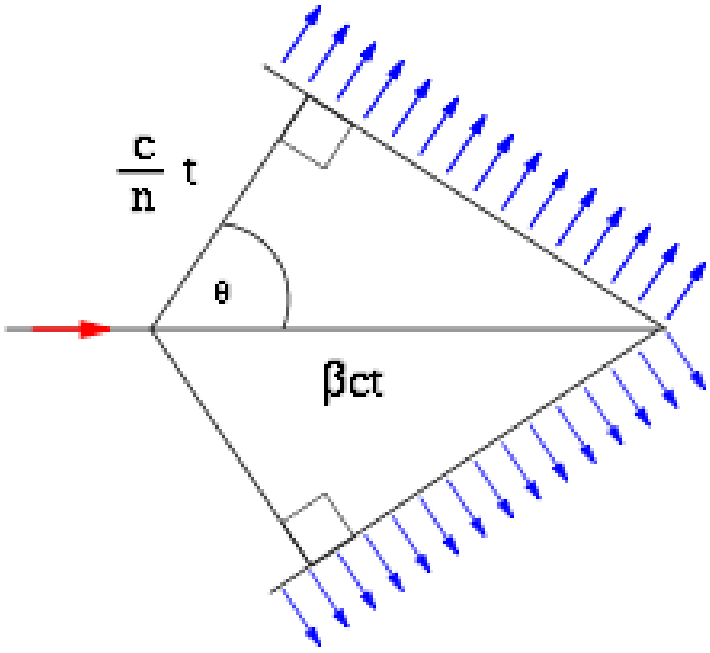

(b) Cherenkov Diagram

The θ angle of the emission cone shown above in the figure **??** and can be calculated with the following equation:

$$\cos\theta = \frac{1}{\beta n} \tag{3.2}$$

When the Cherenkov radiation falls into screen perpendicular to the orbit of the particle, creates a circular ring (Cherenkov rings), its size which depends on its velocity υ particle and screen distance. The cherenkov radiation form a muon produced by a muon neutrino event a well defined cirecular ring in the photomultiplier detector bank. The cherenkov radiation from the electron shower produced by an electron neutrino event produces multiple cones and therefore diffuce ring in the detector array.

In the case of a CC interaction producing a muon [3], this feature can be used to reconstruct the track of the lepton and hence of the original neutrino. Indeed, at high energy one has:

$$\theta_{\mu\nu} \sim \frac{0.6^{\text{deg}}}{\sqrt{E_\nu(TeV}} \tag{3.3}$$

where $\theta_{\mu\nu}$ is the mean angle between the direction of arrival of the neutrino and the track of the muon. The number of photons emitted per unit wavelength interval, dλ, and unit distance traveled, dx, by a charged particle of charge e and of velocity $\beta = \frac{v}{c}$ is given by[15]:

$$\frac{d^2N}{dxd\lambda} = \frac{2\pi}{137\lambda^2}(1 - \frac{1}{\nu^2\beta^2} \tag{3.4}$$

3.3.2 Interaction Signatures

Depending on the neutrino flavour and the type of interaction, three different event signatures are expected in the KM3NeT-ORCA detector.Hadronic showers are resulted, when a high-energy neutrino can recoil a quark and change the original nucleon structure. They interact and decay to create more and more hadrons, resulting in a hadronic shower. This process can happen in every neutrino interaction, apart from the NC channel. Electrons from electron neutrino interactions cause a cascade of photons and electron-positron pairs: an electromagnetic shower. A muon, on the other hand, propagates through the detector with an energy dependent straight path length, and is, thus, referred to as a track [6].

Apart from the Cherenkov radiation, there are alternate ways for losing energy such us ionization, Bremsstrahlung radiation and electron-positron pair production. Ionization is dominant in the low GeV region, but the contribution from Bremsstrahlung 16and pair production increases linearly with energy and is dominant above 1 TeV. The emitted photons through these processes can cause small electromagnetic showers along the track of a muon through pair production or Compton scattering. Tracks, hadronic, and electromagnetic showers are also a signature of tau neutrino interactions, where the tau decays either into a muon, hadron, or electron. These have distinct signatures from the normal interaction due to the time delay in the tau decay, but can be indistinguishable because of the position resolution of the ORCA detector[14].

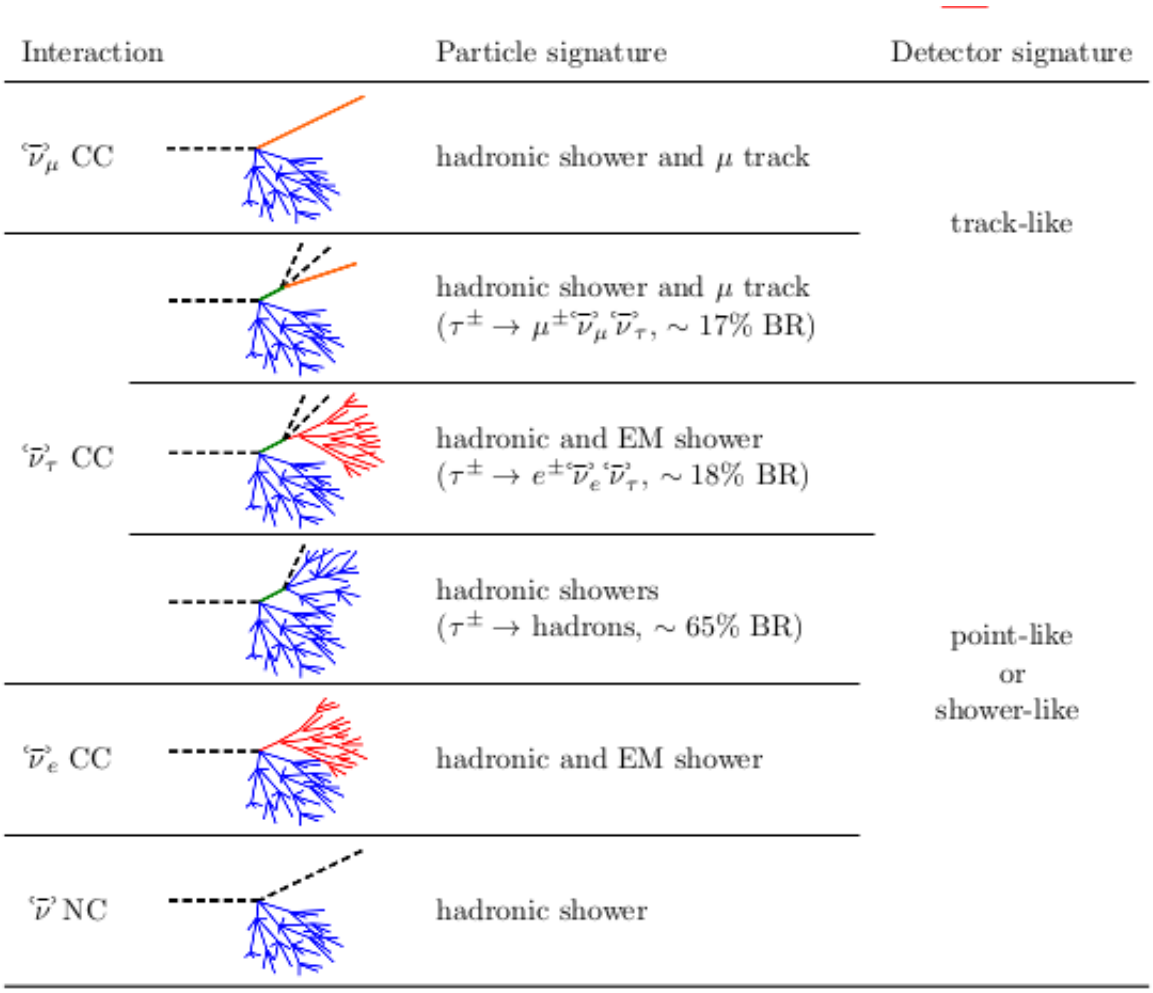

Figure 3.8: The dashed-line represents the different neutrinos. The red line is the muon track. The The tau neutrino (green), the EM shower (blue) and Hadronic shower (red) [14].

3.3.3 Background Sources

Unfortunately, due to the large and natural location of the experiment, several background sources exist that obscure the neutrino signal. In the "uncontrolled" experimental setup of the Mediterranean Sea, exist background sources like the natural radioactive elements, the dark count rate, bioluminescence and atmospheric-muons:

- **K-40 decay**:There are some radioactive isotopes in the sea water that are beta-radioactive. The most dominant source is the isotope Potassium-40, whose electron, can emmit Cherenkov radiation. Furthermore, there are other K-40 decay products, whose secondary products pass the Cherenkov condition.

- **Dark count rate**: Despite darkness, thermal noise can cause the photocathode to produce an electron and result in a false hit.
- **Bioluminescence**: In the Mediterranean Sea, some luminescent creatures exist in the depths of the sea and produce light, through some chemical reactions. This light can be detected by the PMTs of the experiment and thus result in background hits.
- **Atmospheric muons**: The interaction of cosmic radiation with atmosphere molecules can result in the production of muons, neutrinos and other particles that ORCA aims to measure. The Earth is used to provide a shielding, since only neutrinos can travel through the Earth. However, the down-going rate of atmospheric muons is far greater than the atmospheric neutrinos, which makes it difficult to distinguish them without proper reconstruction of track.

3.4 Trigger and Data Acquisition

For Data Acquisition, the "All-data-to-shore" concept is utilized in the KM3NeT detector[4][1], in which all analogue signals that passed a designated threshold are digitised and sent to the shore to be processed in real-time. When a pulse charge on a PMT is over threshold, its analogue signal is digitised into a time (t) and a time-over-threshold (T oT). The combination of these two data values is known as an "L0 hit", also often referred to as just a "hit". Every 100 ms each DOM sends an identically sized time window containing all L0 hits to shore. To maintain time consistency between each DOM, a fibre-optic network, an on-shore White Rabbit switch,and electronics embedded in the DOM work together to synchronise the complete detector 18up to nanosecond precision. The events are filtered, in order to cut background [3.3.3] using designated software and each event will contain a snapshot of all the data in the detector during the event.

After the time slice arrives on-shore over Ethernet,the data stream has to be reduced. Without it, a full building block would result in a stream of 25 Gb/s; much of which is background noise. Therefore due to the large amount of data, the software are required to reduce the total amount by a factor of about 105. They look for N causally related hits from two different PMTs on the same DOM within a 10ns time window (L1 hits). If found, all the L0 hits at the same time as the L1 hits, and those in a time window of approximately 10μs before and after the causally related hits are combined into a single event.

3.4.1 TriggerCPU (TCPU)

The TCPUs[7] are responsabile for the online analysis. This means that each TCPU has the snapshot of the whole detector during a specific TimeSlice. After its creation, each TTS is analyzed with a 2-steps trigger system

- The **Level 1 (L1)** algorithms search for hit coincidences and charge excess along the whole TTS, identifying interesting portions of data, called events, made of the hits occurring in a time window 6 μs-wide centred in the trigger seed. The event window is increased if another trigger condition is satisfied within it.
- The **Level 2 (L2)** algorithms implement more complex conditions that operate on L1 events. If a L2 is satisfied, the event is marked to be saved on permanent storage.

4. ORCA Experiment

The aim of the ORCA experiment is to determine the hierarchy of the neutrino masses. The ordering of neutrino mass eigenstates has indeed not been determined so far. After fixing $m_{21} = (m^2)_{sol} > 0$, two solutions remain possible depending on the sign of m_{31} : the normal hierarchy ($NH : m_1 < m_2 < m_3$) and the inverted hierarchy ($IH : m_3 < m_1 < m_2$). The determination of the NMH is of fundamental importance to constrain the models that seek to explain the origin of mass in the leptonic sector and the differences in the mass spectrum of charged quarks and leptons.

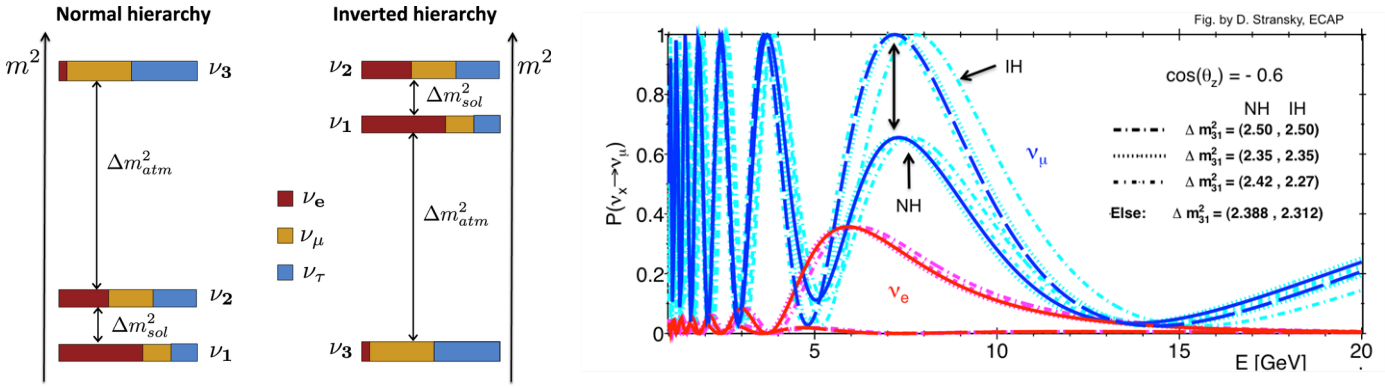

Figure 4.1: Neutrino Mass Hierarchies

The determination of the NMH can be accomplished by studying the neutrino oscillations in the region of a few GeV. The method utilizes the probability and rate of $\nu_\mu <->\nu_e$ in the appearance at the atmospheric mass scale. In the 3ν framewor, the $\nu_\mu <->\nu_e$ and $\nu_\mu <->\nu_\mu$ transition prabability in vacuum can be approximated by the following formulae:

$$P_{3\nu}(\nu_\mu \to \nu_e) \sim \sin^2\theta_{23} * 2\sin^2\theta_{13}\sin^2\frac{\Delta m^2_{31}L}{4E_\nu} \tag{4.1}$$

$$P_{3\nu}(\nu_\mu \to \nu_\mu) \sim 1 - 4\cos^2\theta_{13}\sin^2\theta_{23}(1-\cos^2\theta_{13}\sin^2\theta_{23}) * \sin^2\frac{\Delta m^2_{31}L}{4E_\nu} \tag{4.2}$$

4.1 Propagation of Particles and Light Production

As stated in (neutrino interaction), when particles propagate through the detector volume, the different types of particles must be taken in light production in water:

- Muons that are characterized by long, approximately straight tracks continuously losing energy and emitting Cherenkov photons. They also suffer stochastic losses which produce independent electromagnetic (EM) showers.
- EM showers that are either produced by bremsstrahlung photons from muons or by electrons at the neutrino interaction vertex. All their energy is deposited in a short distance (on the scale of the detector) and can generally be considered point-like. They contain a large number of electrons and hence, statistically, showers of a similar energy all have similar properties
- Hadrons at the neutrino interaction vertex, that have complex decay chains and the amount of light they produce depends on the primary particle and its particular set of decays. In addition, they may produce muons in the final state which may travel a significant distance. Hence, they are not amenable to parametrization in the same way electrons and muons are.

4.2 Track Reconstruction

For a track-like event, the position of the lepton is described by three parameters: x, y, and t. No z position is required due to a degeneracy with the time parameter, t. Similarly, the direction of the lepton can be described a unit vector with two independent angles because of the cylindrical symmetry of the track. Instead of the actual angles, two parameters of the unit vector are used in the reconstruction: dx and dy.

$$\begin{aligned} dz &= \cos\theta \\ dx &= \sin\theta\cos\phi \\ dy &= \sin\theta\cos\phi \end{aligned}$$

where θ and ϕ the zenthal and the azimuthial angles from the z-axis, respectively. All the track parameters are included in the vector $\vec{\theta_{track}}$.

The muon tracks can be difined by five independent parameters: the position of the muon $\mathbf{P} \equiv (p_x, p_y, p_z)$ at a given time and its normalized direction $\vec{d} \equiv (d_x, d_y, d_z)$**??**. Defining $\vec{v} = \mathbf{Q}_i - \mathbf{P}$ as a vector that goes from point $\mathbf{P}$ to the hit position $\mathbf{Q}_i$.

$$P\vec{P}_i = 1 - \frac{\sqrt{\vec{u}^2 - l^2}}{\tan\theta_c} \tag{4.3}$$

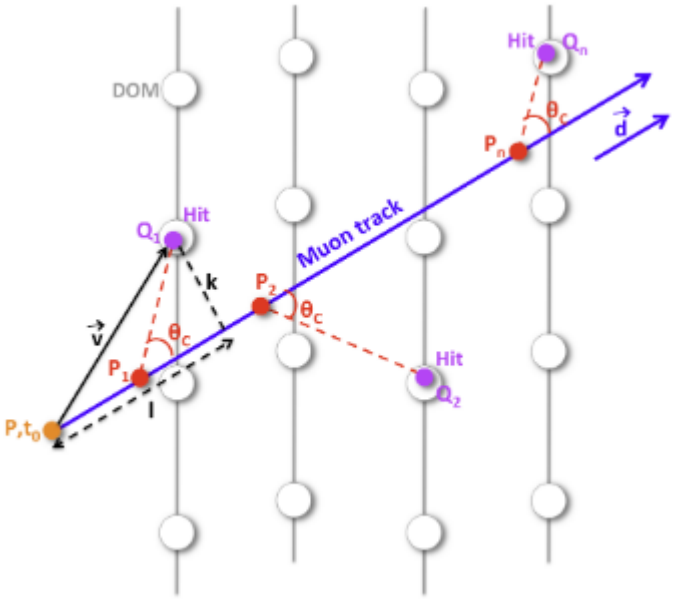

Figure 4.2: Description of the geometry for the detection of Cherenkov light

The reconstruction of track can be divided in two phases, the pre-reconstruction, where the JPrefit library is and main reconstruction. Through these phases the most probable track is given to an event.

4.2.1 Pre-reconstruction: JPrefit

The pre-reconstruction phase, JPrefit, is responsible generating the initial values for the main reconstruction algorithm, JGandalf. By performing a directional scan over the whole sky with 5° between guesses, around 800 tracks are created around the centre of hits. At this stage, the tracks length is assumed to be infinite.

JPrefit[6] utilizes the time information of each hit to create a χ^2 funcition 4.4, in order to asses the viability of each one from the 800 "candidate tracks".

$$\chi^2 = \sum_{i}^{hits} \frac{(t_i - t_c)^2}{\sigma_i^2} \tag{4.4}$$

JPrefit regards the "candidates tracks" as the most plausible, the ones that with its parameters that χ^2 function is minimized. The set consist of the time parameter (t) and two positional parameters orthogonal to the direction of the track: x and y. The three parameters are combined with the direction to give a track guess. The best 36 quality tracks are given to JGandalf, to determine the "best fitted" track.

4.2.2 Main-reconstruction: JGandalf

In the main reconstruction phase the maximum likelihood method is used to determine the event hypothesis that approximate better the observed data. The time of the hits are compared to the probability of light to arrive at that time $P(D_i|\vec{\theta_{track}}))$. JGandalf's likelihood gives the quality of the track and its parameters. This procedure is applied in all 36 given tracks and the highest ranked likelihood of the "candidate" tracks provides the best fitted track parameters.

$$\mathcal{L}(\vec{\theta_{track}}|\vec{D_i}) = \prod_{i=1}^{hits} P(D_i|\vec{\theta_{track}})) \tag{4.5}$$

4.3 Energy Reconstruction

4.3.1 Reconstruction: JEnergy

The algorithm utilizes the best tracks from the main reconstruction-phase, JGandalf algorithm, in order to perform a fit of the muon energy. From the muon trajectory, the energy of the muon can be identified by using the spatial distribution of hit and non-hit PMTs. The probability of a PMT defined as a hit can by expressed as:

$$\mu(\rho, \theta, \phi) \equiv \int_{T_{min}}^{T_{max}} dt \frac{\partial P(\rho, \theta, \phi, r)}{\partial t} \tag{4.6}$$

where $\mu(\rho, \theta, \phi)$ is the number of photo-electrons.

4.4 Reconstruction Limits

Unfortunately, no algorithm can without a doubt recreate the original direction and energy of the neutrino. Several restrictions prevent this from happening, that's why only the muon direction and an energy threshold can be found. However due to the process of scattering, the muon from the neutrino direction can slightly differ. Thus an axiomatic limit is set in the reconstruction phase. The change from quasi-elastic and resonance scattering to deep inelastic scattering opens up the phase space for the muons energy with a larger component going to the shower.

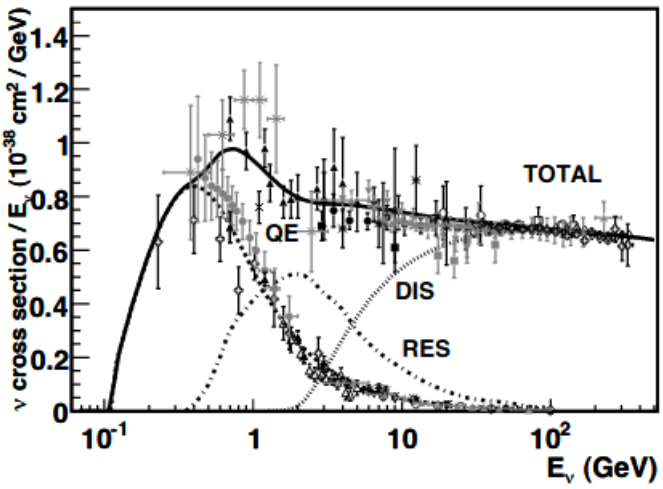

(a) Neutrino Cross Section

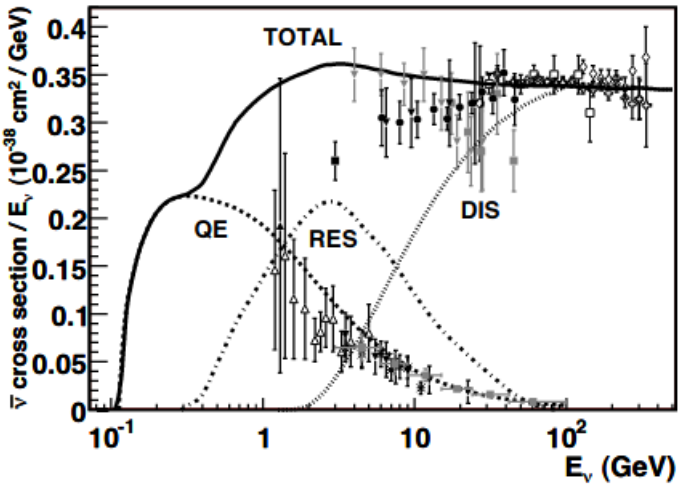

(b) Anti-Neutrino cross section

Figure 4.3: Total neutrino and anti-neutrino per nucleon CC cross sections (for an isoscalar target) divided by neutrino energy and plotted as a function of energy. As dashed the quasi-elastic scattering, as dot-dashed the resonance production and as dotted deep inelastic scattering are presented [10].

5. Neutrino Energy Reconstruction in ORCA6

In this chapter, lies my personal contribution. The studies I have performed focus on the energy resolution for reconstructed muon tracks coming from atmospheric neutrino interactions, for the KM3NeT-ORCA detector configuration of six detection units (ORCA6). For this analysis, Monte Carlo generated neutrino events have been used.

5.1 Energy Reconstruction of ORCA6

As the detection volume of the ORCA6 configuration is very limited, only a part of the muon track traverses the detector for high energy (>100 GeV) muons. As a result, the reconstructed energy is significantly lower than the true energy. In this work, the influence of other event characteristics on the energy resolution is investigated. The following variables are introduced:

- E_r:The reconstructed energy calculated using the PMT hit information (time and charge) as described in subsection 4.3.1.
- E_t: The true neutrino energy, which is known only for Monte Carlo generated neutrinos.

From the Figs: 5.1-5.2, one can observe that:

- In the low energy region (1 - 35 GeV), the energy resolution is satisfactory, although, as can be seen in Fig. 5.2, neutrinos seem to be systematically reconstructed at lower energy than the true (MC) E_ν.
- In the energy region 35 - 80 GeV, a "deep" can be observed in both figures. One of the main goals of this work has been the investigation of the influence of event characteristics to the existence of this deep, other than the limited size of the detector.
- In the medium energy region of 80 - 1000 GeV, there are many different behaviours of the distributions. For reconstructed energy below 30 GeV, we can see a saturation of events, whereas as in the previous "deep" region,there seems a lack of events reconstructed with energies below E_ν $100GeV$. For $E_reco > 100GeV$, there seem to be two different contributions to the E_reco versus E_true distribution.

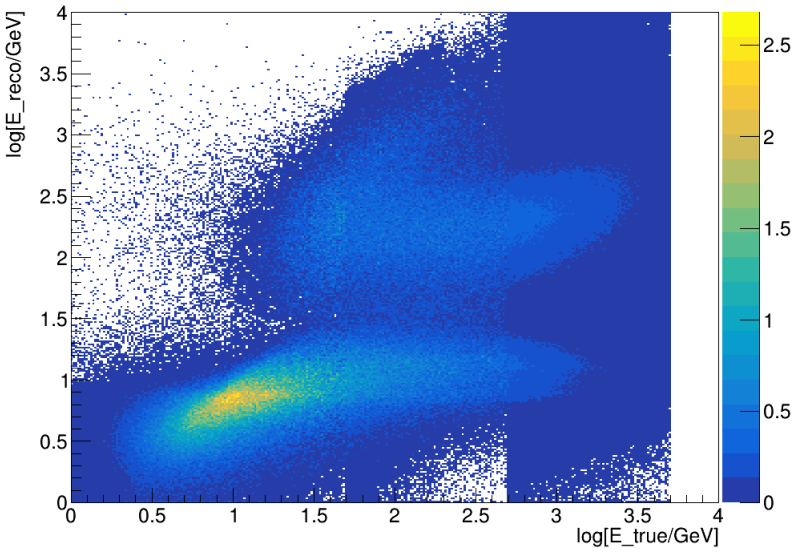

Figure 5.1: Reconstructed versus true neutrino energy.

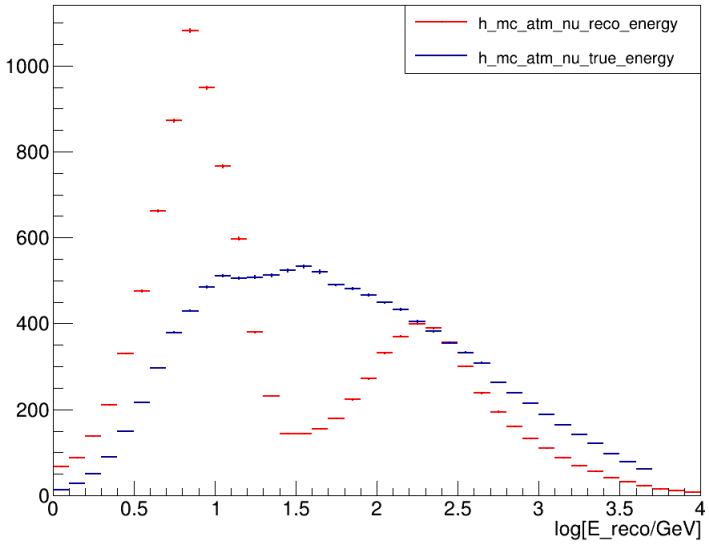

Figure 5.2: Reconstructed neutrino energy (in red) compared to the true neutrino energy (in blue)

- For very high energy neutrinos ($E_\nu > 1$ TeV) the energy reconstruction seems to be reasonable, as they leave adequate light in the detector volume.

- Notice that the discontinuities observed in Fig. 5.1 for E_true $50GeV$ and E_true $500GeV$, are artificial, as they are due to the fact that these values are the exact energy boundaries of the generated root files that have been used for the analysis.

5.2 Analysis Tools

For the analysis, various tools were used:

- analyze_orca_data.cc: ROOT code used for the main analysis
- Event Display: code used to visualize an event. Taken from the KM3NeT group, but configured it in order to visualize and neutrino events.
- pre-processing code: Taken from Dimitris Stavropoulos and used it to generate the root files used for the analysis.

5.2.1 ROOT Framework

ROOT is an object-oriented program and library developed by CERN, mainly used for high energy physics. As high-performance software, ROOT is written mainly in C++. This software enables statistically sound scientific analyses and visualization of large amounts of data.

There are some prerequisites for a successful ROOT run:

- C++ compiler
- Linux Operating System

5.2.2 Familiarization with ROOT

As part of my internship, I had to adapt to the complex nature of ROOT software. Apart from the trainings and the online literature, I was tasked with an assignment in order to familiarize myself with ROOT. I had to integrate the MC random noise event root files, in the analysis. I performed various runs with different conditions, in order to reduce the contribution of the K40 background events (random noise) in the data collected by the detector.

These conditions were the following:

- $no\_doms\_cher\_hit \geq 5$
- $Nhits > 20$
- $log\_lik > 1.7$

From the previous conditions, the following root files were created:

- results.root: no conditions apllied
- results_cher.root: $no\_doms\_cher\_hit > 5$
- results_Nhits.root: $Nhits > 20$
- results_loglik.root: $log\_lik > 1.7$
- results_cher_loglik.root: $(no\_doms\_cher\_hit > 5)\&\&(log\_lik > 1.7)$
- results_cher_Nhits.root:$(no\_doms\_cher\_hit > 5)\&\&(Nhits > 20)$
- results_Nhits_loglik.root: $(Nhits > 20)\&\&(log\_lik > 1.7)$

Note: The root file with all three conditions was not needed, because from the two conditions, the random noise was minimized. The inclusion of an additional condition, would only reduce data events without having a significant suppression to the random noise contribution.

5.3 Analysis

The objective of the analysis is to study the distribution of various variables relating to the topology of the events and the reconstruction of energy. The first impressions are that due to the uneven geometry of the detector (Fig:3.4), the topology would certainly affect the quality of reconstruction. In order to find, if certain characteristics of the event topology affect the precision of the energy reconstruction, different "slices" were created in the True and Reconstructed Energy range.

- True Energy
  - lslice: $10 - 13GeV$
  - deep: $31 - 65GeV$
  - mslice: $100 - 126GeV$
  - hslice: $1 - 1.26TeV$
- Reconstructed Energy
  - le: $E_r < 31GeV$
  - me: $31 < E_r < 65GeV$
  - he: $E_r > 65GeV$

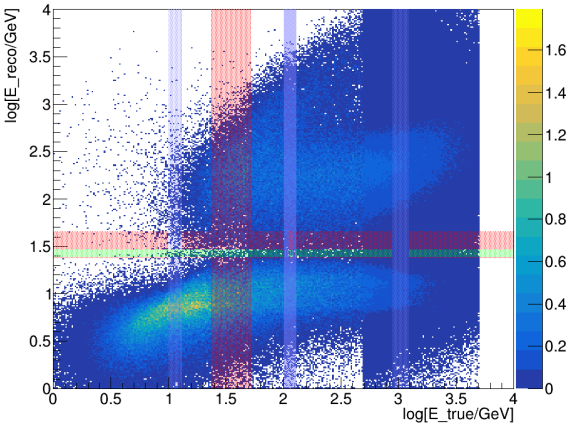

(a) The reconstructed energy versus the true neutrino energy is shown. The energy ranges used for our study are indicated.

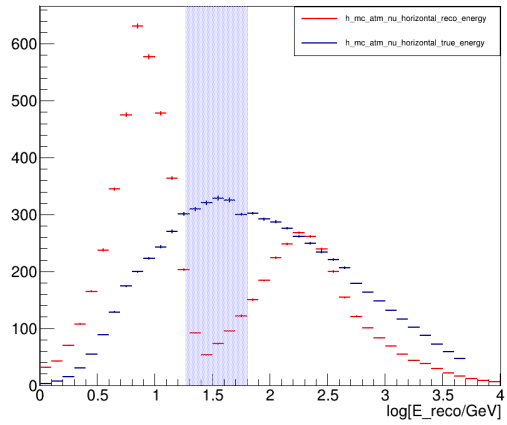

(b) Reconstructed neutrino energy (in red) compared to the true neutrino energy (in blue). The "deep" in the reconstructed energy is indicated with the blue band.

Figure 5.3: The energy ranges which are further investigated are shown.

For each of the listed energy 2d-regions, all of the mentioned variables in the following list, will be examined in order to identify whether or not they contribute to the quality of reconstruction.

- reco zenith
- true zenith
- true phi
- reco phi
- bjorken y
- reco_vrtx_r
- reco_vrtx_z
- d closest
- z closest
- TrackLength
- Nhits

5.3.1 Zenith angle

Zenith is defined as the zenithial angle of the neutrino direction. The start of the angle is designated the South Pole and is measured from 0 to 180 degrees. Depending on the direction of the particles, some sets of data can be categorized as horizontal, up, down, upgoing and downgoing.

For the analysis, even though all events, irrespective of their zenith, were utilized, the focus is put on horizontal events, as they are expected to be mostly affected by the current detector topology Figure 3.4.

Table 5.1: Zenith angle used to indicate the event direction

A/A	Event Direction	Condition
1	Up	$zen > 90^o$
2	Down	$zen < 90^o$
3	Upogoing	$150^o < zen < 180^o$
4	Downgoing	$0^o < zen < 30^o$
5	Horizontal	$60^o < zen < 120^o$

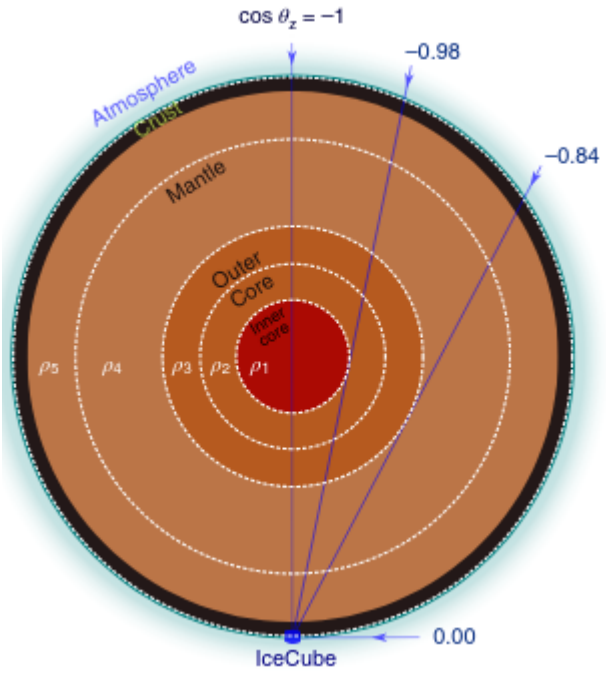

Figure 5.4: Zenith angle distribution

5.4 Event Display

The Event Display code is used for visualization of single events. With this code all the necessary variables are presented, providing a broader look in the peculiarities of each event. The code was provided by the group, but I configured it in order to suit my needs.

```
else if (((reco_energy)<31)&&(true_energy>=31) && (true_energy<=65)&&(indexes_upgoing[2]<1)){
  cout << "For particle inside the Deep Energy-Region for upgoing events, the following identifications:" << endl;
  cout << "With exact True Energy:" << true_energy << "\t Deep Energy-Region Particle with Ereco="<< reco_energy  << endl;
  cout << "True Zenith: " << true_zenith << "\t Zenith Variation:" << abs(zenith-true_zenith) <<"\t Phi:" << true_phi << "\t Phi Variation:" << abs(reco_phi-true_phi) <<endl;
  cout << "Run: " << run << "\t Event ID:" << event_id << "\t Index:" << index << "\t Flav:" << flav << "\t Interaction Type:"<< int(interaction_type)<< "\t Cos_Zen:" << cos_zen << "\t no_hits:"<< no_hits<< endl;
  cout << "Reco_vrtx_z:" << reco_vrtx_z << "\t Reco_vrtx_r:" << reco_vrtx_r << "\t Bjorken y:" << bjorken_y << "\t TrkLength:" << TrkLength << "\t d_closest:" << d_closest << "\t z_closest" << z_closest << "\n" << endl
  indexes_upgoing[2]=indexes_upgoing[2]+1;}
else if ((reco_energy)>31&&(reco_energy<65)&&(true_energy>=31) && (true_energy<=65)&&(indexes_upgoing[3]<1)){
  cout << "For particle inside the Deep Energy-Region for upgoing events, the following identifications" << endl;
  cout << "With exact True Energy:" << true_energy << "\t Deep Energy-Region Particle with Ereco="<< reco_energy << endl;
  cout << "True Zenith:" << true_zenith <<  "\t Zenith Variation:" << abs(zenith-true_zenith) <<"\t Phi:" << true_phi << "\t Phi Variation:" << abs(reco_phi-true_phi) <<endl;
  cout << "Run: " << run << "\t Event ID:" << event_id << "\t Index:" << index << "\t Flav:" << flav << "\t Interaction Type:"<< int(interaction_type)<< "\t Cos_Zen:" << cos_zen << "\t no_hits:"<< no_hits<< endl;
  cout << "Reco_vrtx_z:" << reco_vrtx_z << "\t Reco_vrtx_r:" << reco_vrtx_r << "\t Bjorken y:" << bjorken_y << "\t TrkLength:" << TrkLength << "\t d_closest:" << d_closest << "\t z_closest" << z_closest << "\n" << endl
  indexes_upgoing[3]=indexes_upgoing[3]+1;}
else if (((reco_energy)>65)&&(true_energy>=31) && (true_energy<=65)&&(indexes_upgoing[4]<1)){
  cout << "For particle inside the Deep Energy-Region for upgoing events, the following identifications:" << endl;
  cout << "With exact True Energy:" << true_energy << "\t Deep Energy-Region Particle with Ereco="<< reco_energy  << endl;
  cout << "True Zenith: " << true_zenith << "\t Zenith Variation:" << abs(zenith-true_zenith) <<"\t Phi:" << true_phi << "\t Phi Variation:" << abs(reco_phi-true_phi) <<endl;
  cout << "Run: " << run << "\t Event ID:" << event_id << "\t Index:" << index << "\t Flav:" << flav << "\t Interaction Type:"<< int(interaction_type)<< "\t Cos_Zen:" << cos_zen << "\t no_hits:"<< no_hits<< endl;
  cout << "Reco_vrtx_z:" << reco_vrtx_z << "\t Reco_vrtx_r:" << reco_vrtx_r << "\t Bjorken y:" << bjorken_y << "\t TrkLength:" << TrkLength << "\t d_closest:" << d_closest << "\t z_closest" << z_closest << "\n" << endl
  indexes_upgoing[4]=indexes_upgoing[4]+1;}
```

Figure 5.5: Event Display Code

```
For particle inside the Deep Energy-Region for horizontal events, the following identifications:
With exact True Energy:32.0858   Deep Energy-Region Particle with Ereco=205.888
True Zenith: 88.9574     Zenith Variation:4.208  Phi:23.6365     Phi Variation:0.814783
Run: 7397        Event ID:11     Index:147       Flav:-14        Interaction Type:1      Cos_Zen:-0.0552189      no_hits:97
Reco_vrtx_z:21.1717      Reco_vrtx_r:37.8347     Bjorken y:0.999862      TrkLength:55.2218       d_closest:4.1153        z_closest23.2516
```

Figure 5.6: Event Display Print-Out

The main root code has a special part added (Fig:5.5), which provides the necessary information such us the event id, the run id for running the event display code. When running the main code all the desired variables are printed for a single event (Fig:5.6) and these variables have also been used to verify that the code to select the events is correct.

6. Results

The analysis is completed for all the energy and zenith ranges. Although as stated in the report (Section:5.1 and Section:5.3.1), the horizontal events and the "deep" region are the most important for understanding the effect of the event characteristics on the precision of energy reconstruction, due to limited space only this region will be presented.

6.1 "Deep" Region

As stated in the section 5.3, the "deep" region is an energy range, for which the energy resolution is poor; these events seem to be reconstructed at significantly lower energies. The event distributions of associated variables are presented, for all events in the "deep" region with true neutrino energy 30 - 80 GeV, which are 1) reconstructed with smaller energy, 2) reconstructed with $E_r/simE_t$ and 3) for events with $E_r > E_t$. for particles that are reconstructed with smaller energy than their true, for particles with similar E_r and E_t and for events that $E_r > E_t$.

To ease the compilation of the figures, the same colour code is used in all the plots that follow:

- Blue: Events that are reconstructed with lower energy than the true neutrino energy (from MC)
- Green: Events that are reconstructed with similar energy than the true neutrino energy (from MC)
- Red: Events that are reconstructed with higher energy than the true neutrino energy (from MC)

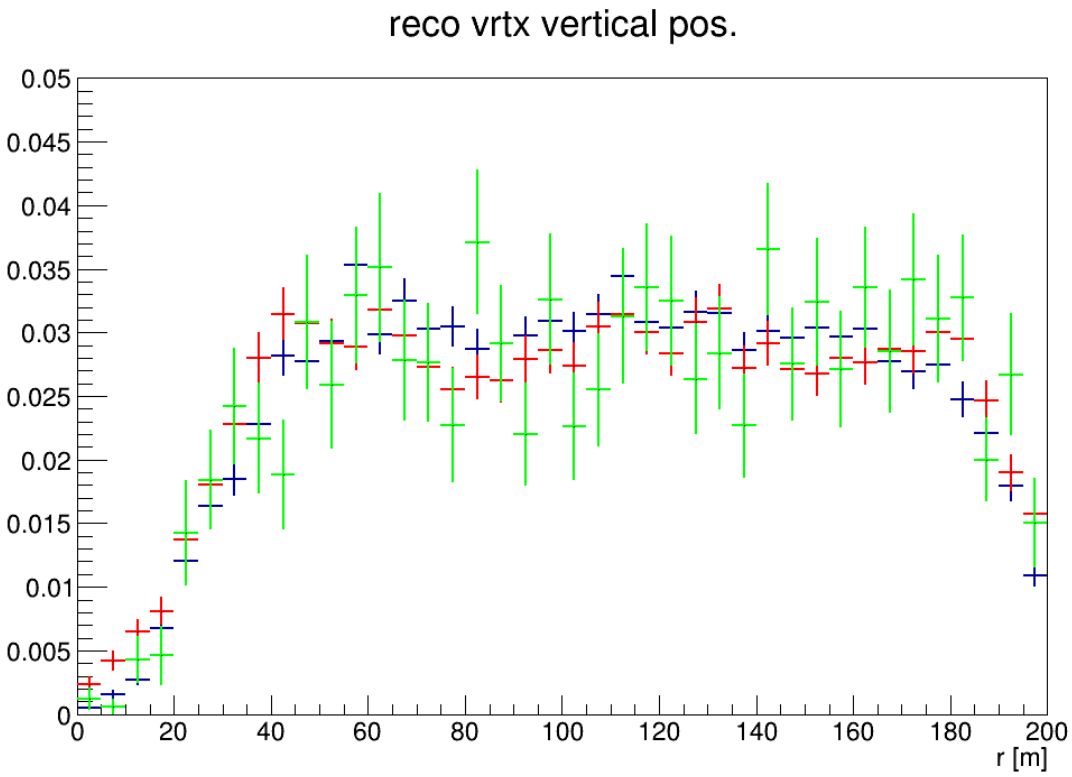

(a) *reco_vrtx_z*

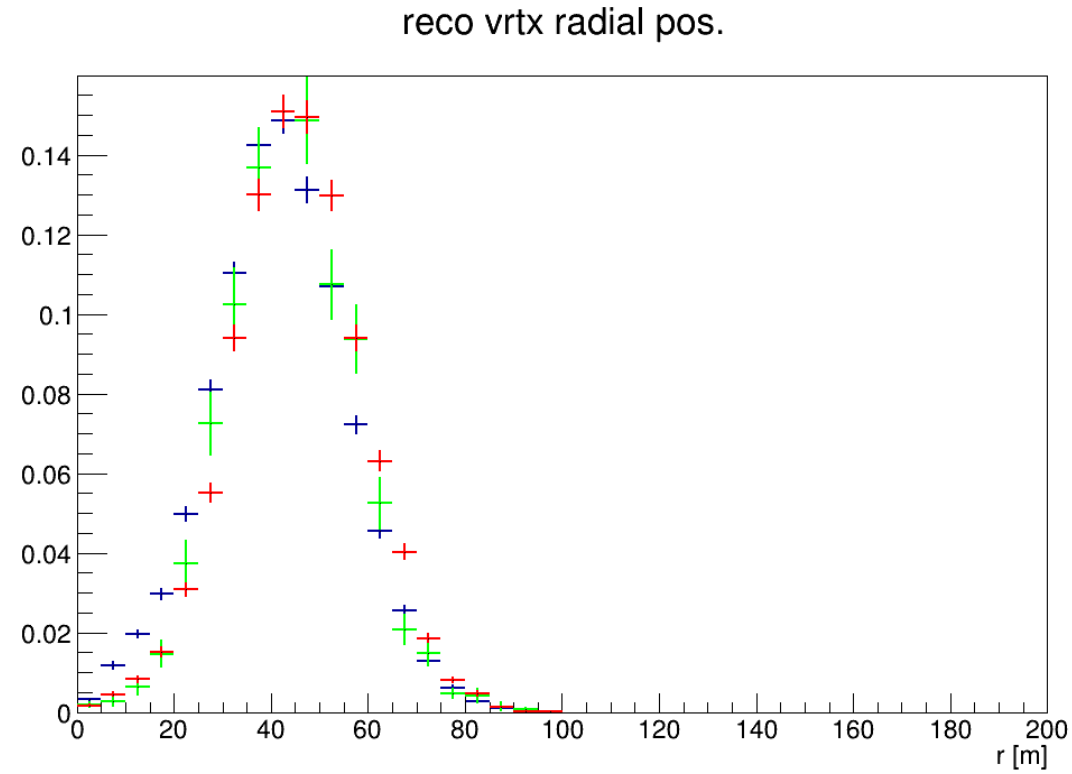

(b) *reco_vrtx_r*

Figure 6.1: Reconstruction of Vertex

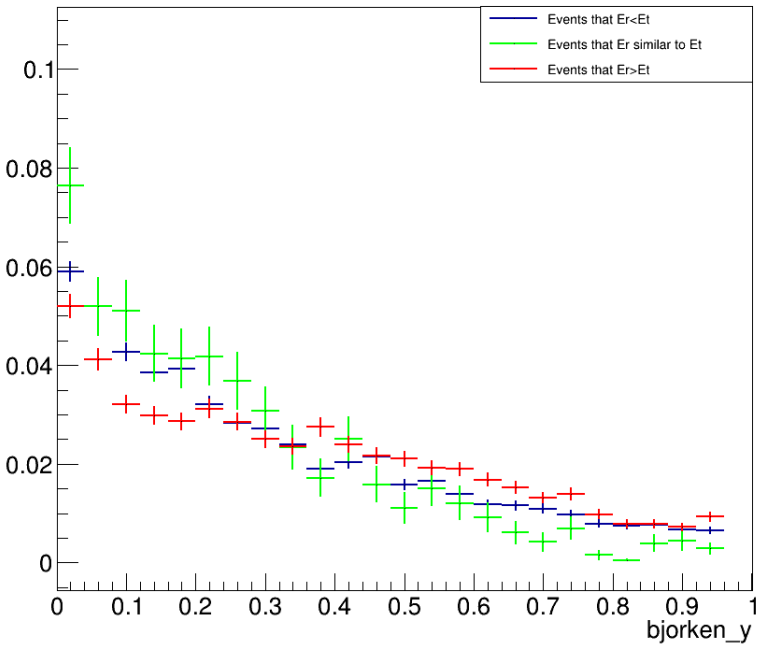

Figure 6.2: Bjorken y

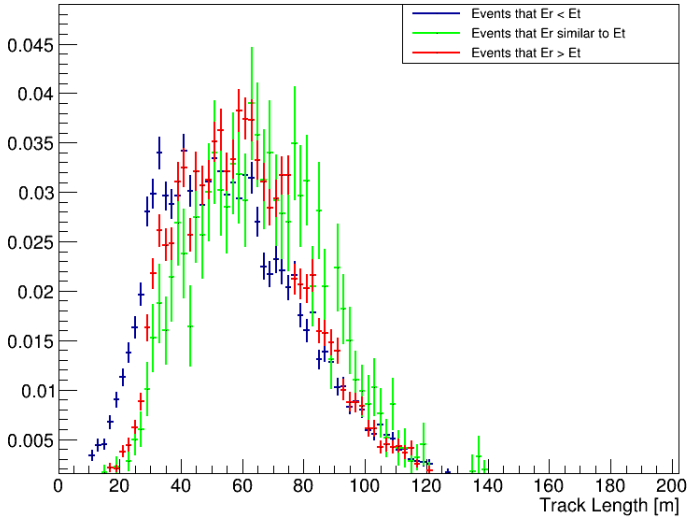

Figure 6.3: Track Length

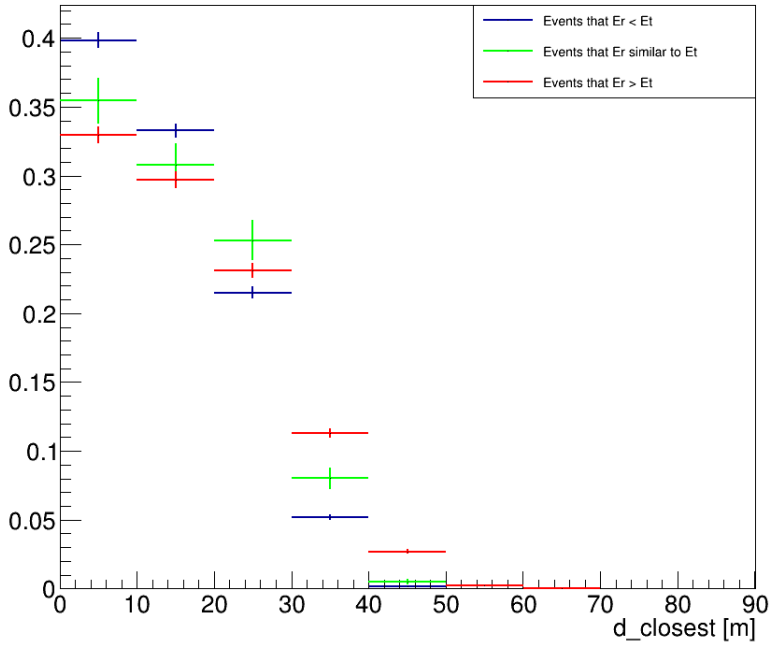

(a) *d_closest*

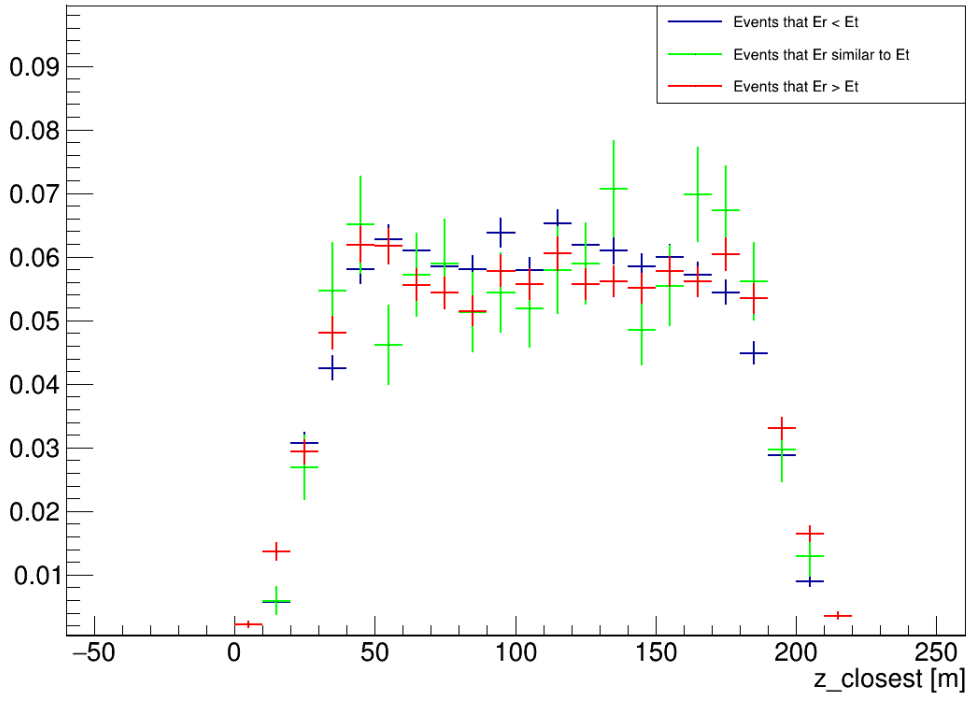

(b) *z_closest*

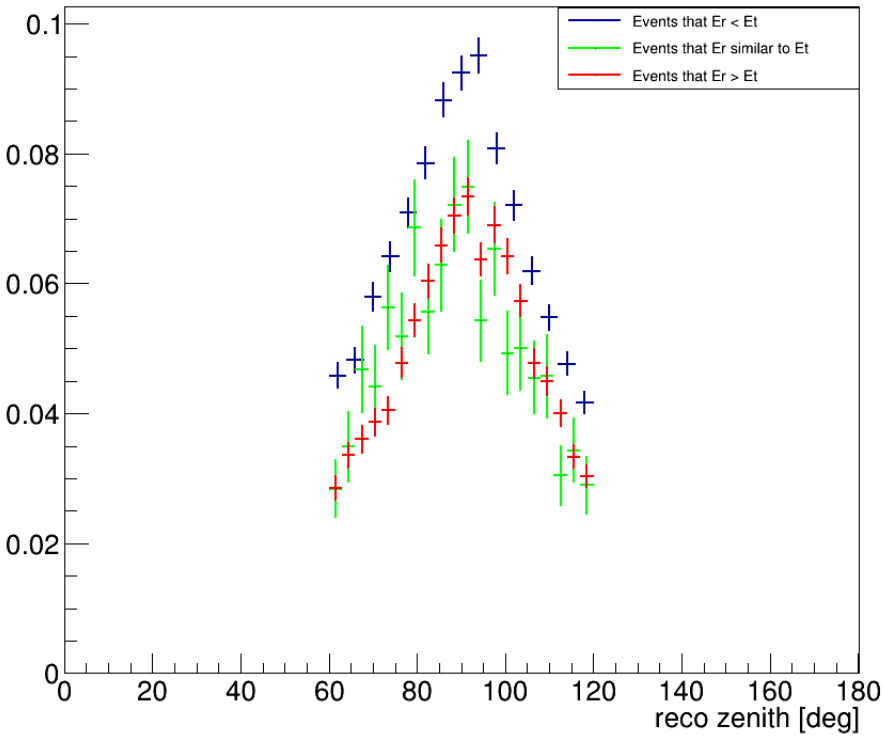

Figure 6.5: zenith angle

6.2 Event Display

In this section three events will be visualized, that represent the three different types of events depending on the difference between the true and reconstructed energy. Furthermore for each event a xy and rz plot was created, in order to complement the event display.

6.2.1 Event ID: 56 Run ID: 7397

This event is reconstructed with energy similar to its true.

- $E_t = 11.86$ GeV
- $\Delta\phi = 21.56^o$
- $TrkLength = 45.12m$
- $E_r = 10.97$ GeV
- $no\_hits = 105$
- $zenith = 163.58^o$
- $reco\_vrtx\_r = 4.31m$
- $d\_closest = 0.89m$
- $\Delta zenith = 1.67^o$
- reco_vrtx_z= 147.91m
- $\phi = -165.65^o$
- $bjorken\_y = 0.1$
- $z\_closest = 160.81m$

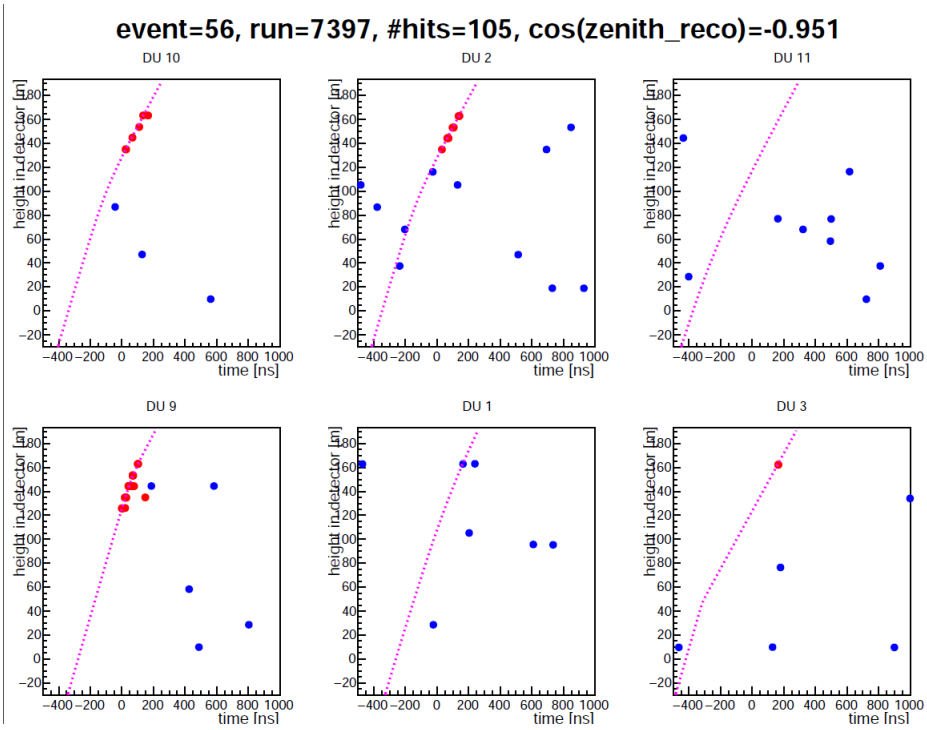

Figure 6.6: Event Display ID:56

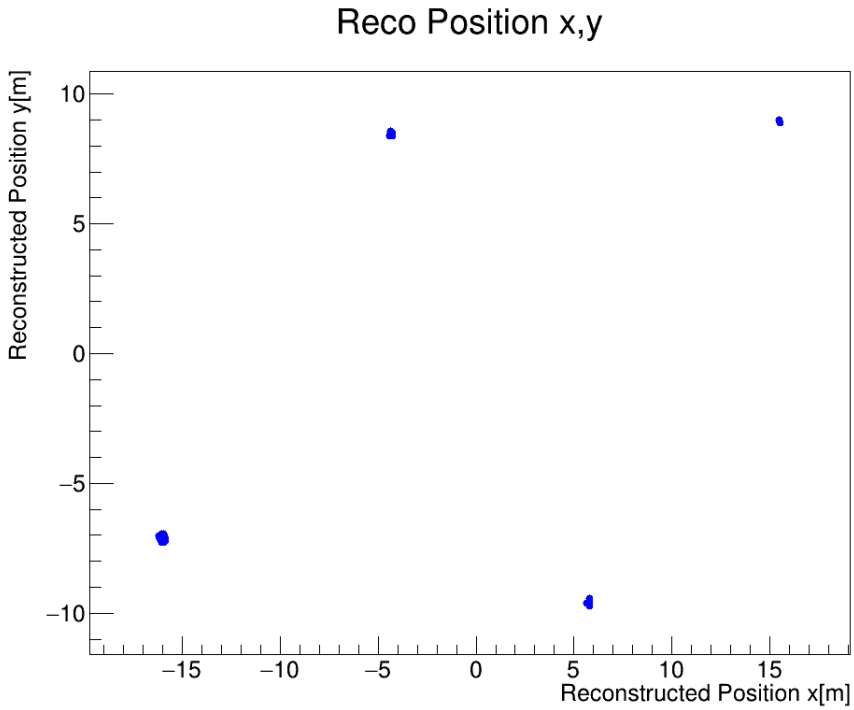

Figure 6.7: xy plot ID:56

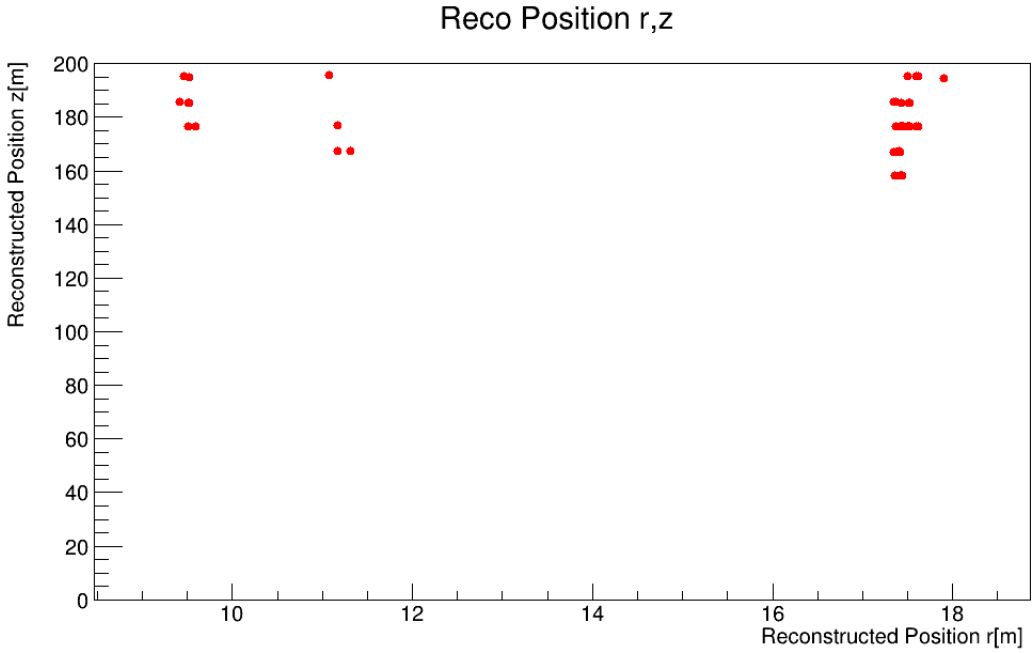

Figure 6.8: rz plot ID:56

6.2.2 Event ID: 60 Run ID: 7397

This event is reconstructed with energy lower to its true.

- $E_t = 34.03$ GeV
- $E_r = 21.06$ GeV
- $zenith = 69.44^o$
- $\Delta zenith = 3.35^o$
- $\phi = 150.44^o$
- $\Delta\phi = 6.75^o$
- $no\_hits = 121$
- $reco\_vrtx\_r = 60.48m$
- reco_vrtx_z=152.19m
- $bjorken\_y = 0.29$
- $TrkLength = 85.60m$
- $d\_closest = 1.18m$
- $z\_closest = 133.47m$

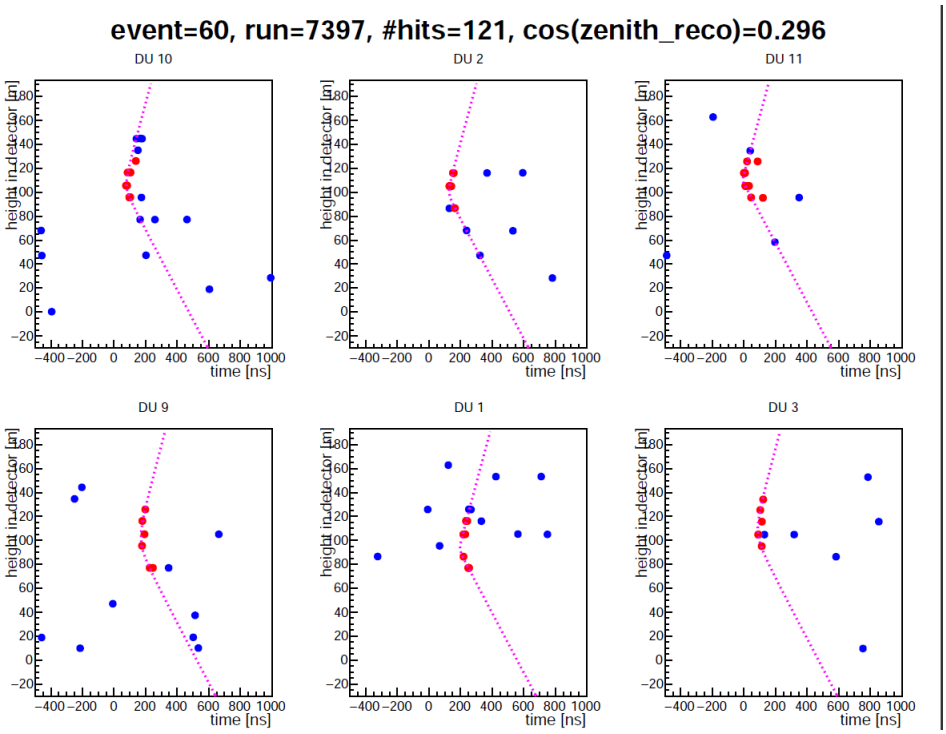

Figure 6.9: Event Display ID:60

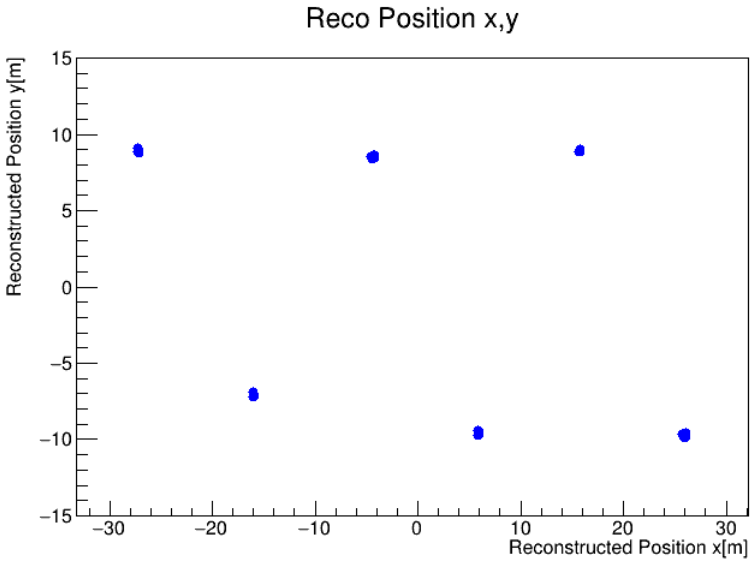

Figure 6.10: xy plot ID:60

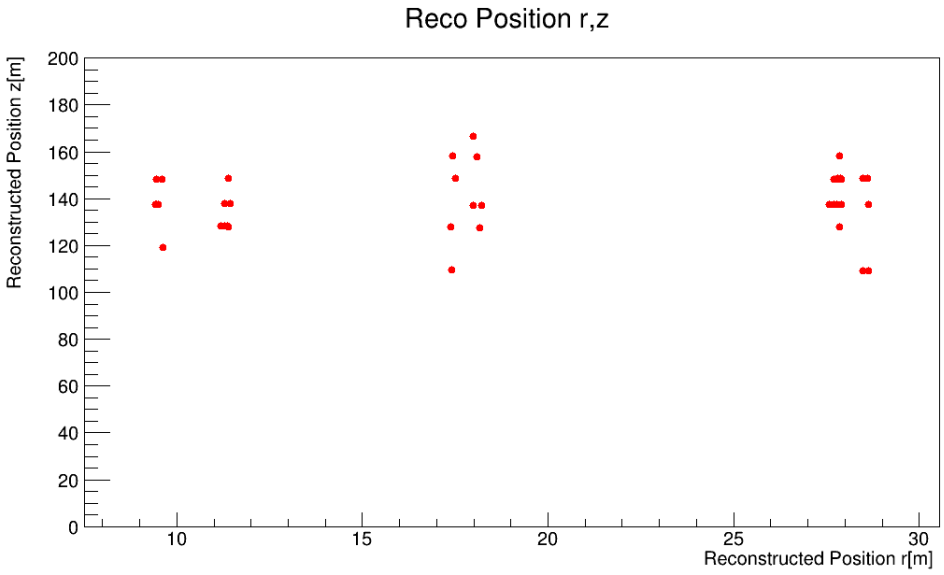

Figure 6.11: rz plot ID:60

6.2.3 Event ID: 255 Run ID: 7397

This event is reconstructed with energy much higher than its true.

- $E_t = 11.34$ GeV
- $E_r = 173.99$ GeV
- $zenith = 108.74^o$
- $\Delta zenith = 6.05^o$
- $\phi = 53.95^o$
- $\Delta\phi = 0.68^o$
- $no\_hits = 93$
- $reco\_vrtx\_r = 36.09m$
- reco_vrtx_z=183.31m
- $bjorken\_y = 0.99$
- $TrkLength = 22.75m$
- $d\_closest = 5.26m$
- $z\_closest = 199.81m$

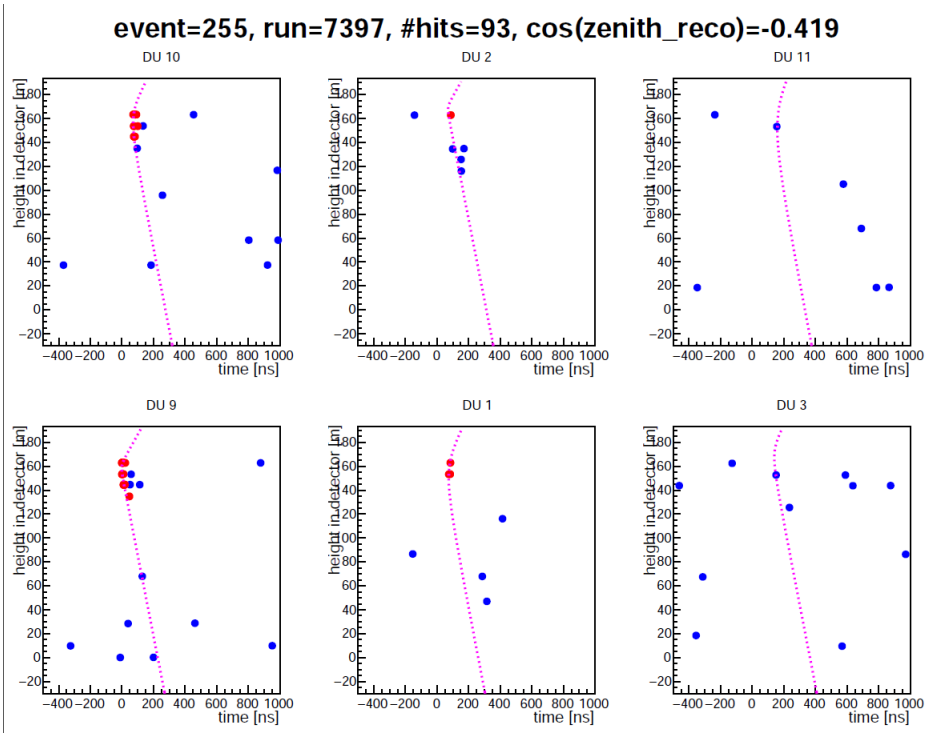

Figure 6.12: Event Display ID:255

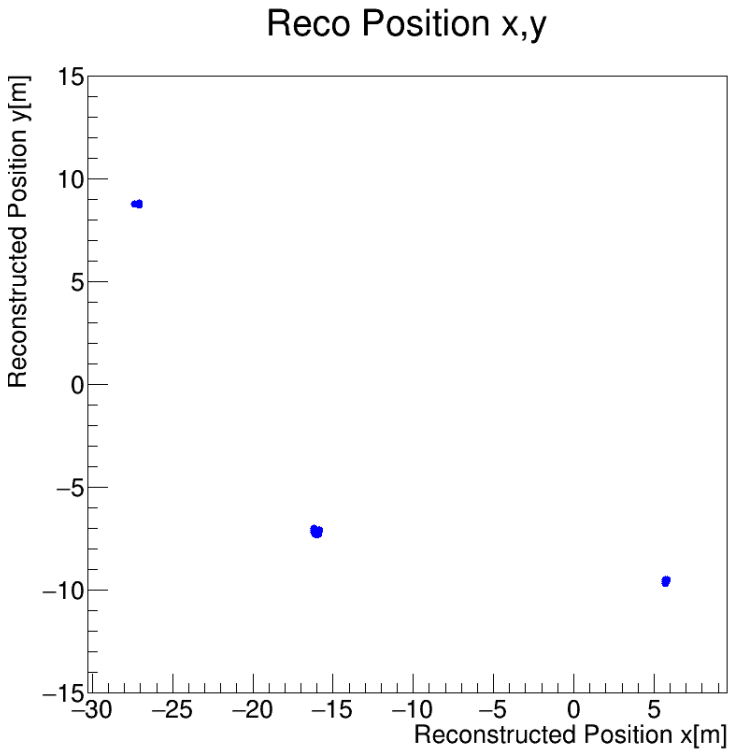

Figure 6.13: xy plot ID:255

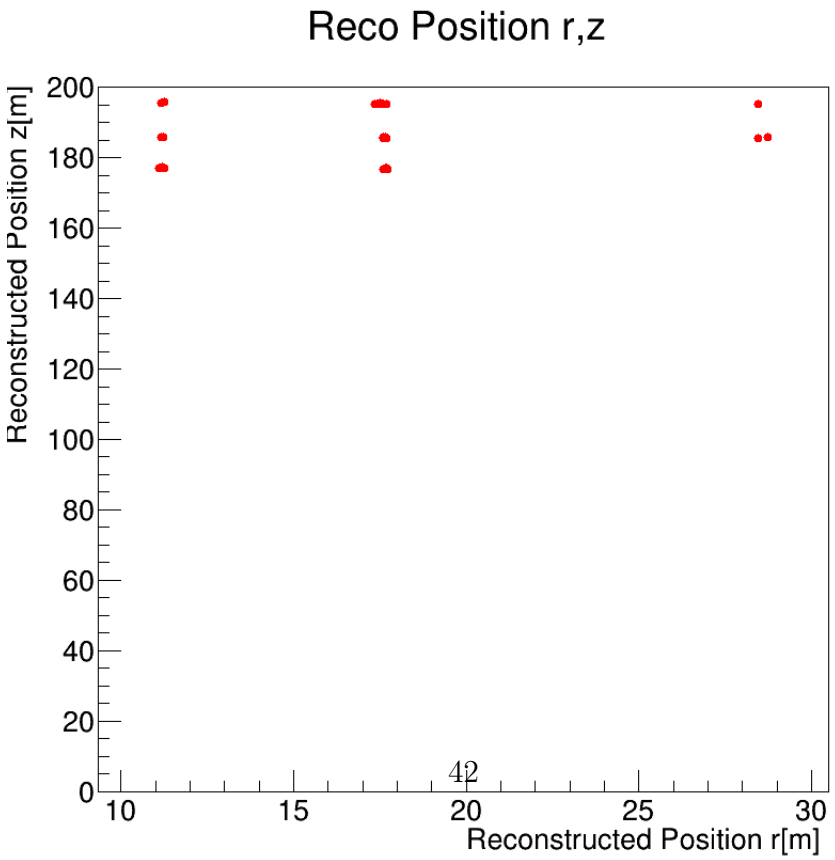

Figure 6.14: rz plot ID:255

7. Discussion Conclusion

Given the limited size of the KM3NeT-ORCA detector, the energy reconstruction is a very challenging task. In this report, a detailed study for the quality of the energy reconstruction of muonic neutrinos for the ORCA6 detector has been made.

7.1 Event Display

7.1.1 Event ID:255

For the event with id:255, it is clear that due to its trigger in the outer DOMs of the detector the reconstruction is overestimated. The event doesn't have enough track length inside the detector to properly estimate its energy. Also, it is clear from reco vertex that the event vertex is outside the detector.

7.1.2 Event ID:56

For the event with id:56, the detector collects trigger and cherenkov hits with 4 of its strings, Furthermore, the no of hits and the track length is sufficient enough to reconstruct accurately the energy. Also, it is clear from reco vertex that the event vertex is outside the detector.

7.1.3 Event ID:60

For the event with id:60, even though ORCA detects trigger and cherenkov hits from all the strings, the no of hits and the track length is sufficient enough, somehow the reconstruction of energy is not properly accomplished. This event is extremely interesting, because it defies the norms and from what we know it should have been reconstructed with its appropriate energy.

7.2 Deep Region

From the various variable distributions (**Figs:6.1**), it is clear that the position of the reconstructed vertex does not have a significant impact of the goodness of the energy reconstruction.

Furthermore, there is no evidence of correlation between bjorken y (**Fig:6.2**) or the zenith (**Fig:6.5**) and the quality of the energy reconstruction. On the other hand, from (**Figs:6.4a & 6.4b**), indicate a correlation with the accuracy of the energy reconstruction. Especially, for the d_closest we can see that for events with $d\_closest < 30m$, the events that are a non-negligible fraction of events are reconstructed with lower energies. However for values above 30, there is a sharp decline and events reconstructed with higher energies dominate. In particular, for events with d_closest above 50m, almost all events are reconstructed with higher energy. The z_closest distribution also indicates a possible correlation with the goodness of the energy reconstruction. From, in the **Fig:6.3** it is clear that events reconstructed with lower energy populate mostly the region of small track lengths, although there is a significant tail towards larger values of the track length.

7.3 Conclusion

From the analysis, a clear correlation of the goodness of the energy reconstruction with the distance of closest approach to the detector is found. The limited detection volume certainly has an impact to the energy reconstruction. Also, at the time of this study, there was not information for the shower part of the event, a significant asset, but because of the limited time of the internship it was not feasible in regards of the timeline. In conclusion, the results of this work can be used as input to future studies.

A. Code

The code is uploaded as part my own repository in **GitLab**. Due to using work from other members of KM3NeT group, I don't have the authority to publish my versions of the code. However I can upload all the results produced by my study.

Bibliography

[1] S. Adrián-Martínez, M. Ageron, F. Aharonian, S. Aiello, A. Albert, F. Ameli, E. Anassontzis, M. Andre, G. Androulakis, M. Anghinolfi, and et al. Letter of intent for km3net 2.0. *Journal of Physics G: Nuclear and Particle Physics*, 43(8):084001, Jun 2016.

[2] G. Barenboim, P. B. Denton, S. J. Parke, and C. A. Ternes. Neutrino oscillation probabilities through the looking glass. *Physics Letters B*, 791:351–360, 2019.

[3] B. Baret and V. V. Elewyck. High-energy neutrino astronomy: detection methods and first achievements. *Reports on Progress in Physics*, 74(4):046902, apr 2011.

[4] S. Biagi, T. Chiarusi, P. Piattelli, and D. REAL. The data acquisition system of the KM3NeT detector. In *Proceedings of The 34th International Cosmic Ray Conference — PoS(ICRC2015)*, volume 236, page 1172, 2016.

[5] S. Bourret. *Neutrino oscillations and earth tomography with KM3NeT-ORCA*. PhD thesis, APC, Paris, 2018.

[6] M. M. Briel. *Muonic event reconstruction in KM3NeT-ORCA*. PhD thesis, University of Amsterdam, 2019.

[7] T. Chiarusi, M. Favaro, F. Giacomini, M. Manzali, A. Margiotta, and C. Pellegrino. The trigger and data acquisition system for the KM3net-italy neutrino telescope. *Journal of Physics: Conference Series*, 898:032042, oct 2017.

[8] M. Circella. The Digital Optical Module -DOM- of the KM3NeT detector. In *33rd International Cosmic Ray Conference*, page 1223, 2013.

[9] C. L. Cowan, F. Reines, F. B. Harrison, H. W. Kruse, and A. D. McGuire. Detection of the free neutrino: a confirmation. *Science*, 124(3212):103–104, 1956.

[10] J. A. Formaggio and G. P. Zeller. From ev to eev: Neutrino cross sections across energy scales. *Reviews of Modern Physics*, 84(3):1307–1341, Sep 2012.

[11] M. K. Gaillard, P. D. Grannis, and F. J. Sciulli. The standard model of particle physics. *Reviews of Modern Physics*, 71(2):S96–S111, Mar 1999.

[12] D. Gangopadhyay and A. Sinha Roy. Three flavoured neutrino oscillations and the leggett garg inequality. *The European Physical Journal C*, 77, 02 2017.

[13] M. M. S. J. e. a. Gonzalez-Garcia, M.C. Global fit to three neutrino mixing: critical look at present precision. *J. High Energ. Phys.*, 24:093006, Nov 2012.

[14] J. Hofestädt. *Measuring the neutrino mass hierarchy with the future KM3NeT/ORCA detector*. doctoralthesis, Friedrich-Alexander-Universität Erlangen-Nürnberg (FAU), 2017.

[15] J. V. Jelley. Cerenkov radiation: Its origin, properties and applications. *Contemporary Physics*, 3(1), 10 1961.

[16] A. Markus, H. Klaus, and P. de los Heros Carlos. Detection of the free neutrino: a confirmation. *Probing particle physics with IceCube*, 78(924):103–104, 2018.

[17] L. Nauta et al. First neutrino oscillation measurement in KM3NeT/ORCA. *PoS*, ICRC2021:1123, 2021.

[18] X. Qian and P. Vogel. Neutrino mass hierarchy. *Progress in Particle and Nuclear Physics*, 83:1–30, 2015.

[19] A. Sinopoulou, R. Coniglione, R. Muller, and E. Tzamariudaki. Atmospheric neutrinos with the first detection units of km3net/arca. *Journal of Instrumentation*, 16(11):C11015, Nov 2021.

[20] M. Thomson. *Modern particle physics*. Cambridge University Press, New York, 2013.